HHS Public Access

Author manuscript

Circ Res. Author manuscript; available in PMC 2022 April 30.

Published in final edited form as:

Circ Res. 2021 April 30; 128(9): 1279–1296. doi:10.1161/CIRCRESAHA.120.318458.

Innervation and Neuronal Control of the Mammalian Sinoatrial Node: A Comprehensive Atlas

Peter Hanna[1,2], **Michael J. Dacey**[1,2], **Jaclyn Brennan**[3], **Alison Moss**[4], **Shaina Robbins**[4], **Sirisha Achanta**[4], **Natalia P. Biscola**[5], **Mohammed A. Swid**[1], **Pradeep S. Rajendran**[1], **Shumpei Mori**[1], **Joseph E. Hadaya**[1], **Elizabeth H. Smith**[6], **Stanley G. Peirce**[6], **Jin Chen**[8], **Leif A. Havton**[5,9,10], **Zixi (Jack) Cheng**[8], **Rajanikanth Vadigepalli**[4], **James Schwaber**[4], **Robert L. Lux**[1], **Igor Efimov**[3], **John D. Tompkins**[1], **Donald B. Hoover**[6,7], **Jeffrey L. Ardell**[1,2], **Kalyanam Shivkumar**[1,2]

[1]University of California Los Angeles (UCLA) Cardiac Arrhythmia Center and Neurocardiology Research Program of Excellence, Department of Medicine

[2]UCLA Molecular, Cellular & Integrative Physiology Program, UCLA

[3]Bioengineering, George Washington University, Washington, DC

[4]Daniel Baugh Institute for Functional Genomics/Computational Biology, Department of Pathology, Anatomy, and Cell Biology, Thomas Jefferson University, Philadelphia, PA

[5]Neurology, Icahn School of Medicine at Mount Sinai, New York City, NY

[6]Biomedical Sciences

[7]Center of Excellence in Inflammation, Infectious Disease and Immunity, James H. Quillen College of Medicine, East Tennessee State University

[8]University of Central Florida, Burnett School of Biomedical Sciences, College of Medicine, Orlando, FL

[9]Neuroscience, Icahn School of Medicine at Mount Sinai, New York, NY

[10]VA RR&D National Center of Excellence for the Medical Consequences of Spinal and; Cord Injury and Neurology Service, James J. Peters Veterans Administration Medical Center, Bronx, NY

Address correspondence to: Dr. Kalyanam Shivkumar, 100 UCLA Medical Plaza, Suite 660, Los Angeles, CA 90095, Tel: 310-206-6433, kshivkumar@mednet.ucla.edu.

DISCLOSURES

University of California, Los Angeles has patents developed by K.S. and J.L.A. relating to cardiac neural diagnostics and therapeutics. K.S., J.L.A. and P.S.R. are co-founders of NeuCures, Inc.

SUPPLEMENTAL MATERIAL

Expanded Methods
Tables I-V
Figures I-XI
Movies I-VI

Abstract

Rationale: Cardiac function is under exquisite intrinsic cardiac neural control. Neuroablative techniques to modulate control of cardiac function are currently being studied in patients, albeit with variable and sometimes deleterious results.

Objective: Recognizing the major gaps in our understanding of cardiac neural control, we sought to evaluate neural regulation of impulse initiation in the sinoatrial node (SAN) as an initial discovery step.

Methods and Results: We report an in-depth, multiscale structural and functional characterization of the innervation of the SAN by the right atrial ganglionated plexus (RAGP) in porcine and human hearts. Combining intersectional strategies including tissue clearing, immunohistochemical and ultrastructural techniques, we have delineated a comprehensive neuroanatomic atlas of the RAGP-SAN complex. The RAGP shows significant phenotypic diversity of neurons while maintaining predominant cholinergic innervation. Cellular and tissue-level electrophysiological mapping and ablation studies demonstrate interconnected ganglia with synaptic convergence within the RAGP to modulate SAN automaticity, atrioventricular conduction and left ventricular contractility. Using this approach, we comprehensively demonstrate that intrinsic cardiac neurons influence the pacemaking site in the heart.

Conclusions: This report provides an experimental demonstration of a discrete neuronal population controlling a specific geographic region of the heart (SAN) that can serve as a framework for further exploration of other parts of the intrinsic cardiac nervous system (ICNS) in mammalian hearts and for developing targeted therapies.

GRAPHICAL ABSTRACT

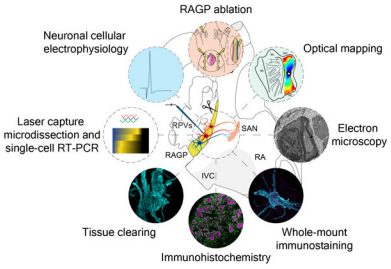

Keywords

autonomic nervous system; electrophysiology; neuroanatomy; neurophysiology; sinoatrial node

Subject Terms:

Arrhythmias; Autonomic Nervous System; Electrophysiology; Gene Expression and Regulation; Physiology

INTRODUCTION

The nervous system intricately regulates almost every aspect of cardiac physiology and profoundly influences pathophysiological adaptions to disease[1]. Cardiac autonomic control

is achieved by a nuanced interplay between the extra-cardiac neural circuits that interface with the intrinsic cardiac nervous system (ICNS), the clusters of ganglia found in ganglionated plexuses (GPs) in epicardial fat pads on the surface of the heart. These GPs contain afferent and efferent neurons that transduce information from and to the myocardium as well as local circuit neurons[2, 3]. The ICNS coordinates cardiac reflexes in concert with inputs from the hierarchy of the cardiac neuraxis composed of cortical centers, brain stem, spinal cord and intrathoracic sympathetic ganglia and may serve as a nexus point for therapies for cardiovascular disease[3].

Understanding the control of the ICNS on discrete cardiac regions has implicated specific GPs with certain aspects of cardiac functions. For example, a GP in the intercaval region at the dorsal aspect of the right atrium (RA), known as the right atrial GP (RAGP), has been shown to mediate vagal influences over the sinoatrial node (SAN)[4–7]. Following the description of the human ICNS, a series of comparative anatomic studies show that the RAGP is conserved among mammalian species with fibers originating from the epicardial fat pad and coursing toward the SAN[7]. It is now recognized that GPs do not merely serve as relay stations housing postganglionic parasympathetic neurons, but as integration centers that are interconnected to affect cardiac function[8].

Clinically, there has been recent interest in neuroablative and neuromodulatory interventions at the level of the ICNS. For example, botulinum neurotoxin has been shown to reduce arrhythmia recurrence when injected into the ICNS in one study with 3-year follow-up[9]. In contrast, the neuroablative approach evaluated in the AFACT study (Atrial Fibrillation Ablation and Autonomic Modulation via Thoracoscopic Surgery) did not demonstrate improved arrhythmia recurrence-free survival and, unfortunately, was associated with increased pacemaker implantation rates[10]. Furthermore, while histological studies in the past have been suggestive of neural pathology in the setting of cardiovascular disease such as sudden death[11], disruption of parasympathetic nerves has also been shown to increase ventricular arrhythmogenesis in a murine model[12]. Given the eagerness to perform neurointerventions for arrhythmias in the clinical setting with varying and sometimes deleterious effects, we set forth to perform foundational work to provide a guide to intrinsic cardiac neuroanatomy and physiological control.

Advancing our knowledge of the neural circuits controlling the cardiac impulse origin at the SAN is a logical neural-visceral link to explore the function of the ICNS. Recent advances in characterizing peripheral neural circuits will aid in elucidating the intrinsic cardiac neural control of cardiac function, and here we apply these techniques to understanding the interactions between RAGP and SAN[13]. Because rodent cardiac ganglia do not appear as organized into discrete GPs as in higher-order mammals and the study of large animal models is advantageous in translational arrhythmia research, we chose the Yucatán minipig as a large animal model[14–17]. In this study, we use a multidisciplinary approach to develop in-depth phenotypic and functional assessments of the ultrastructural to macroscopic neuroanatomic connections between the RAGP and SAN in porcine and human tissues.

METHODS

Data Availability.

An expanded methods section is available in the Data Supplement. All protocols and data supporting findings in this study are available in the National Institutes of Health's (NIH) Stimulating Peripheral Activity to Relieve Conditions (SPARC) Data Portal and from the corresponding author upon reasonable request.

RESULTS

Neuroanatomy and Vascular Supply of the RAGP.

The RAGP is located at the dorsal aspect of the intercaval region and lateral to the right pulmonary vein complex in both pig and human (Figure 1). A discrete epicardial fat pad containing the RAGP could be reliably found in porcine and donor human cardiac tissues, and histological examination illustrated that ganglia are found suspended within adipose tissue as well as close to the fat-RA muscle interface (Figure 1B, C, G, and H and Movie I in the Data Supplement). To visualize the neural tissues in 3 dimensions, we applied a tissue clearing technique, immunolabeling-enabled 3-dimensional Imaging of Solvent-Cleared Organs, to generate optically transparent tissue for large volume imaging[13, 18, 19]. iDISCO+-clearing of the porcine and human RAGP and immunostaining with pan-neuronal marker PGP9.5 (protein gene product 9.5) demonstrates that numerous ganglia, found across the thickness of the RAGP fat pad, are interconnected by nerve fiber bundles (Figure 1D, I–K and Movies II through IV in the Data Supplement). We injected the SANs of 2 pigs with neural tracer *FAST* DiI to assess for direct projections from the RAGP to the SAN (Figure 1A). When evaluated after 3 weeks to allow for tracer transport, we observed robust labeling of neurons and nerve fibers in the RAGP and, in many cases, several neuronal processes were evident on individual neurons (Figure 1E). Three weeks was deemed sufficient as labeling of neurons within the right stellate ganglion was identifiable (Figure I in the Data Supplement). The extent of DiI labeling was consistent between pigs, with 21.5% of PGP9.5-positive neurons labeled in one animal and 24% labeled in the other. These neurons were distributed in ganglia across the depth of the RAGP with an enrichment of SAN-projecting neurons at the aspect of the RAGP closest to the SAN (Figure 1F). Injection of contrast media into the right coronary artery of a human cadaveric specimen followed by microCT imaging confirmed that the vascular supply of the RAGP is via the sinus nodal branch of the right coronary artery (Figure 1L and Movie V in the Data Supplement).

Macroscopic and Cellular Organization of the Porcine RAGP.

Most of the ganglia are in the adipose tissue near the atrial muscle and between superficial muscle layers (Figure 2A–D). The typical fat pad has surface dimensions of approximately 2 × 1.5cm and penetrates to a depth of ≈ 1.5 to 2 cm. Ganglia are present throughout the depth of the fat pad and vary in size, containing from 3 to almost ≈170 neurons with substantial variation in size of neurons with cross-sectional area ranging from 599.0 to 3766 μm^2 (Figure 2E–H). Single representative sets of sections from the RAGP fat pad contained from around 750 to 1500 neurons, and the estimated total number of neurons per RAGP ranged from 6000 to 12000.

In contrast to ganglia of smaller species like the mouse, cardiac ganglia of the pig contained primarily multipolar neurons (Figure IIA and IIB in the Data Supplement). Each neuron is surrounded by satellite glial cells that also envelop intraganglionic nerve processes (Figure IIC through IIE in the Data Supplement). Additionally, some ganglia and other sites in the fat pads contained clusters of small intensely fluorescent cells (Figure III in the Data Supplement). Transmission electron microscopy studies of porcine RAGP demonstrated an organizational structure where the RAGP is divided into several distinct compartments and separated by fibrous tissues (Figure IIF through III in the Data Supplement). Ganglionic neurons were present in small clusters that also included satellite cells as well as myelinated and unmyelinated fibers.

Neurons in the Porcine RAGP and Synaptic Inputs to the Ganglia Are Primarily Cholinergic.

We evaluated whether neurons in the porcine RAGP exhibit a cholinergic phenotype and receive extensive cholinergic input from presumed preganglionic vagal efferent nerve fibers. This was confirmed using a well-validated antibody to the VAChT (vesicular acetylcholine transporter; Tables I and II in the Data Supplement), a specific cholinergic marker. The antibody labeled about 99% of the neural cell bodies in the RAGP and revealed intense, punctate staining of presumed preganglionic nerve varicosities in the ganglionic neuropil (Figure 3A through 3C and Figure IVA through IVD in the Data Supplement). Double staining for VAChT and pan-neuronal marker MAP2 (microtubule-associated protein 2) showed that many of these varicosities are found near neuronal cell bodies and their processes.

Some Neurons in Porcine RAGP Express Noncholinergic Neurotransmitter Markers.

We evaluated neurochemical coding of the porcine RAGP (n=4, 2 males and 2 females) in a series of double and triple labeling experiments. Staining for VAChT and TH showed that about 13% of the cholinergic neurons also contain the noradrenergic marker TH (Figure 3D through 3F), consistent with prior studies in other animal models[20], and a small percentage of neurons expressed TH without VAChT. However, most TH-positive neurons lacked staining for VMAT2 (vesicular monoamine transporter 2; Figure 3D and Figure IVE and IVF in the Data Supplement), which is essential for the storage and release of norepinephrine. This contrasts with noradrenergic neurons of the stellate ganglion, which stain intensely for both TH and VMAT2 (Figure VA through VC in the Data Supplement). Nevertheless, a single ganglion with noradrenergic neurons was identified in the RAGP from one out of four pigs evaluated. This ganglion was innervated by VAChT-positive cholinergic nerve fibers and contained typical noradrenergic neurons that stained for TH, VMAT2 and NPY (neuropeptide Y; Figure VD through VL in the Data Supplement). Double labeling of RAGP for TH and NPY showed that 84% of ganglionic neurons showed granular staining for NPY (Figure 3E and 3F and Figure IVG–IVH in the Data Supplement). While TH-positive nerve fibers were abundant in nerve fiber bundles, only scattered nerve fibers within the ganglia stained for TH or NPY. Such fibers appeared to pass through or ramify within the ganglia, occasionally passing close to neurons (Figure 3E). However, neither TH nor NPY was localized to varicose nerve fibers that surrounded RAGP neurons.

We also evaluated the expression of nNOS (neuronal nitric oxide synthase), somatostatin, and VIP (vasoactive intestinal peptide). While we did not detect any neurons expressing somatostatin or VIP, nNOS was expressed in 3% of the neurons evaluated (Figure VIA through VIE in the Data Supplement). No nerve fibers staining for nNOS were detected within ganglia or nerve bundles of the RAGP.

Neurons of Porcine RAGP Are Not Surrounded by Sensory Nerve Fibers Containing Calcitonin Gene-Related Peptide and Substance P.

Innervation of intrinsic cardiac neurons by putative nociceptive sensory nerve fibers that contain CGRP (calcitonin gene-related peptide) and SP (substance P) have been identified in a wide range of species, including humans[21]. Frequently, varicose nerve fibers staining for these neuropeptides surround the intrinsic cardiac neurons, providing prominent innervation [21]. Although porcine RAGP contains many nerve fibers that stain for CGRP and SP, most of these occur in nerve bundles that connect to the ganglia. Relatively few CGRP- or SP-positive nerve fibers enter the ganglia, and only a few of these single fibers pass close to intrinsic cardiac neurons (Figure VIF through VII in the Data Supplement).

Cholinergic Innervation Is More Abundant Than Noradrenergic Innervation in the SAN but Not in RA Myocardium.

We examined the innervation pattern of the SAN and adjacent RA myocardium. Immunolabeling-enabled 3-dimensional imaging of solvent-cleared organs-cleared porcine SAN stained with PGP9.5 showed dense innervation of the SAN with several ganglia identified in the SAN region as well as larger fibers along the longitudinal axis of the crista terminalis (Figure 4A and 4B and Movie VI in the Data Supplement). The SAN region identified by anatomic landmarks was confirmed using serial sections and 3,3′-diaminobenzidine staining with immunostaining for pacemaker channel HCN4 (hyperpolarization-activated cyclic nucleotide-gated channel 4; Figure VIIA in the Data Supplement) and for the periphery of the SAN region with connexin 43, a marker of working myocardium (Figure VIIB in the Data Supplement). Dense cholinergic innervation was noted in this area (Figure VIIC in the Data Supplement). HCN4 staining did not work well with immunofluorescence (Figure VIIIA and VIIIB in the Data Supplement), but we were able to delineate the SAN region by assessing for *HCN4* transcripts using RNA fluorescence in situ hybridization (Figure VIIIC through VIIIE in the Data Supplement). Staining for VAChT and TH showed that cholinergic nerves were more abundant than noradrenergic nerves in the porcine SAN (Figure 4C and Figure VIID and VIIE in the Data Supplement), but both nerve types had comparable density in atrial myocardium (Figure 4D and Figure VIIF and VIIG in the Data Supplement). Quantitative evaluation of nerve density in confocal images from these regions established that cholinergic nerve density is about 5-fold higher than noradrenergic nerve density in the SAN (13% [8.5–16] versus 2.4% [1.5–2.7], adjusted P=0.085) and is significantly less in contractile atrial muscle (1.3% [0.65–2.2], adjusted P=0.006; Figure 4G). Noradrenergic nerve density was more uniform between regions (2.4% [1.5–2.7] in the SAN versus 3.0% [2.0–4.6]) in the atrium, adjusted P>0.99). Since some neurons in the RAGP contained VAChT and TH, we wanted to determine if TH also occurred in cholinergic nerves in the SAN or RA. Colocalization analysis showed that this was not the case (VAChT/TH in SAN versus VAChT/TH in atrium). However, double

labeling for TH and NPY showed that these markers were often colocalized in the SAN (Figure 4E and Figure VIIH and VIII in the Data Supplement) and adjacent RA (Figure 4F and Figure VIIJ and VIIK in the Data Supplement). Quantitative evaluation of staining for TH and NPY showed that the density of nerve fibers for each marker did not differ in SAN (3.3% [1.7–4.1] NPY versus 3.2% [1.7–3.5] TH) and NPY-positive fibers (4.1% [2.4–5.5]) were slightly more abundant than TH-positive fibers (2.3% [1.5–4.1]) in RA, although this was not statistically significant (P=0.49; Figure 4H). These markers were highly colocalized in both regions with 40% (25–53) colocalization of NPY/ TH in SAN (versus VAChT/TH, adjusted P=0.030) and 32% (27–43) in the atrium (versus VAChT/TH, adjusted P=0.15; Figure 4I). Nerves containing NOS, VIP, or CGRP/SP were not detected in the SAN or adjacent RA. Examination of blood vessels in stained sections of the SAN and RA demonstrated prominent perivascular innervation by cholinergic and noradrenergic nerve fibers (Figure IXA through IXD in the Data Supplement). The noradrenergic nerves also contained NPY. Perivascular nerves lacked nNOS and VIP but did contain CGRP and SP (Figure IXE and IXF in the Data Supplement).

Diverse Adrenergic and Cholinergic Receptor Gene Expression in RAGP.

To supplement the above neurochemical coding, we performed a stochastic sampling of RAGP neurons for gene expression profiling. Four hundred five neurons across 4 pigs (2 males and 2 females), mainly close to the posterior RA wall, were sampled and underwent high-throughput polymerase chain reaction (PCR) to evaluate the compilation of neurotransmitter receptors and ion channels expressed (Figure 5A and 5B). Pan-neuronal markers were used as positive controls for the RAGP neurons (Table V in the Data Supplement), which demonstrated a heterogeneity in the peptidergic, adrenergic, and cholinergic, both nicotinic and muscarinic, receptor profiles (Figure 5C). In addition to the diverse expression of sodium, calcium, and potassium channel genes, genes encoding the HCN2 channels, typically found in nociceptive neurons, and HCN4 channels, which mediate I_h in neurons and I_f in the pacemaker cells of the heart, are expressed in RAGP neurons (Figure 5C through 5G). While SP and CGRP were not identified by immunohistochemical methods in RAGP neurons, sensory marker SP (*TAC1*) and its receptor (*TACR1*) are highly expressed in *HCN2*- positive cells (Figure 5D and 5E). Interestingly, in addition to pan-neuronal markers, neurotransmitters, and nicotinic receptors, *HCN2* gene expression was correlated with that of *HCN4*, which may suggest heteromerization of these proteins to form channels (Figure 5F and 5G).

Ultrastructural Imaging and Cellular Electrophysiological Recordings Demonstrate Synaptic Convergence and Nicotinic Transmission.

In contrast to rodent intrinsic cardiac neurons, porcine RAGP neurons lack synaptic inputs to their somata (Figure 6A and 6B). Instead, synaptic contacts are present on dendritic arbors (Figure 6C through 6E). The synaptic boutons show primarily round clear synaptic vesicles with the presence of occasional dense-core vesicles. To characterize these synaptic inputs, we performed cellular electrophysiological measurements. We recorded from a total of 29 neurons isolated from 10 animals (5 males and 5 females). Mean resting membrane potential was −58±7 mV with input resistance of 95±54 MΩ. Most cells (93%, 27/29) were phasic in

nature, firing only a single action potential in response to intracellular injection of depolarizing current (100–500 pA), while 2 cells fired 2 to 4 action potentials.

Stimulation of interganglionic nerves produced bothsubthreshold and suprathreshold excitatory postsynaptic potentials. In 16 ganglion preparations, excitatory postsynaptic potentials were elicited by stimulation of 2 discrete nerve trunks demonstrating a convergence of inputs onto single cells. In 8 preparations, increasing stimulus intensity or duration at a single site recruited multiple inputs resulting in an increased amplitude of the excitatory postsynaptic potential and greater synaptic efficacy (Figure 6F through 6I). In 5 preparations, treatment with the ganglion nicotinic antagonist hexamethonium (500 μmol/L) inhibited the nerve evoked potentials (Figure 6J and 6K).

Ablation of the RAGP Mitigates Vagal Nerve Stimulation-Induced Bradycardia.

To determine the control of the RAGP on cardiac function, the RAGP was ablated in 7 animals (4 males and 3 females; Figure 7A and 7B). Following ablation, resting heart rate (HR) decreased from 100.5±6.9 to 95.7±7.5 bpm (P=0.031) but corrected sinus node recovery time did not significantly change going from 106.9±50.4 to 105.0±26.8 ms (paired t test, P=0.92; Figure 7C). Ablation of the RAGP mitigated right cervical vagal nerve stimulation (VNS)-induced bradycardia from 38.0±8.2% to 5.9±8.3% (P=0.0002) and left cervical VNS-induced bradycardia from 30.0±5.5% to 5.6±8.6% (P=0.001; Figure 7D, upper). In addition to impacting sinoatrial rate, RAGP ablation abolished VNS-induced reductions in left ventricular (LV) contractility from 23.2±5.5% to 5.2±7.5% (P=0.0004) for right cervical VNS and from 31.7±17.0% to 7.3±5.4% for left cervical VNS (P=0.014; Figure 7D, lower). RAGP ablation reduced right stellate ganglion stimulation (SGS)-induced tachycardia from 32.2±18.4% to 25.5±14.2%, but this was not statistically significant (P=0.066). Left SGS does not cause a significant tachycardia at baseline (3.4±3.4%), and this was unchanged by RAGP ablation (2.3±3.2%, P=0.53). Similarly, RAGP ablation did not significantly impact SGS-induced increases in LV contractility (Figure 7D, lower). RAGP ablation reduced right cervical VNS-induced prolongation of atrial-His interval, a measure of atrioventricular conduction, from 56.0±34.4% to 6.0±4.0% (P=0.015; Figure 7E). In contrast, left cervical VNS-induced prolongation was not significantly affected, decreasing from 113.3% (79.5–133.3) to 50.2% (30.1–109.8; P=0.13). VNS-induced changes in ventricular activation-recovery interval, a surrogate marker of action potential duration, with concurrent atrial pacing did not significantly change following RAGP ablation (Figure X in the Data Supplement).

RAGP Stimulation Predominantly Induces Sinus Bradycardia and Pacemaker Shift.

At the macroscopic level, electrical stimulation of the RAGP was performed in a series of *in vivo* porcine experiments (n=8; 6 males and 2 females). Stimulation of the RAGP was initially performed in pigs after bilateral cervical vagotomies, but it was generally difficult to elicit a response under these conditions. However, after complete decentralization with debranching from the vagosympathetic trunk, we were able to elicit at least a 10% bradycardia in 5 of 8 pigs from 88.7 bpm (80.3–113.5) to 73.2 bpm (57.3–100.0), including profound atrioventricular block (P=0.008; Figure 8A through 8C). Additional effects of RAGP stimulation included initial bradycardia followed by return to baseline and increase to

HR with uptitration of frequency during bipolar electrical stimulation, atrial fibrillation (AF) with slow ventricular response and increase in LV pressure with minimal HR increase (Figure XIA and XIB in the Data Supplement). In addition to AF, electrical noise during highfrequency stimulation precluded analysis of atrial-His prolongation on intracardiac electrograms. Atrial electrograms were recorded using multielectrode arrays but because of the large contribution of surrounding contractile myocardium to the electrogram, we were unable to ascertain shifts in pacemaker site (Figure XIC through XIE in the Data Supplement). For this reason, ex vivo optical mapping of a human RAGP-SAN preparation was performed to assess nodal optical action potentials. Based on the vascular supply of the RAGP described above, a wedge preparation of the RAGP-SAN was maintained by coronary perfusion of the right coronary artery. Optical activation maps before and after RAGP stimulation, on tissue from a 52-year-old female human heart, showed an increase in HR from 49 to 113 bpm with 100 Hz stimulation and a superior shift in the pacemaker site (Figure 8D through 8F). These data demonstrate the complexity of the ICNS neural network that underlies the stimulating electrode.

DISCUSSION

We present a comprehensive assessment of the intrinsic cardiac neural control of the impulse origin in the mammalian heart. Using a multiscale approach, we demonstrate (1) interconnected ganglia spanning the RAGP fat pad supply the SAN with an enrichment of neurons close to the SAN; (2) predominantly cholinergic innervation of the SAN yet with heterogeneity in gene and protein expression profiling to identify putative neuronal subpopulations; and (3) the RAGP mediates primarily bilateral vagal inputs to exert profound functional control of the SAN and the leading pacemaking site as well as the atrioventricular node (AVN) and LV.

Within the paradigm of GPs acting as local control centers that serve specific cardiac regions, the RAGP has been postulated as exerting influence over the SAN. While prior studies have suggested RAGP neurons supply the SAN[22], the presence of SAN-projecting neurons throughout the RAGP was confirmed and quantified with the in vivo injection of a neural tracer at the porcine SAN. We were able to apply a tissue clearing technique to perform large volume imaging in porcine and human cardiac tissues to illustrate the dense neural network found in the RAGP fat pad with ganglia distributed throughout the adipose tissue as well as embedded in the posterior RA wall. This finding helps inform the epicardial versus endovascular approaches to targeting the GPs for arrhythmia treatment. We also identified distinct ganglia in the porcine SAN region, which has previously been variably described in the mouse, rat, guinea pig, cat, dog, and human, but whose function have yet to be elucidated[20, 23–26]. Prior descriptions of catecholaminergic cells in ganglia near the SAN raise the possibility that these ganglia are involved in phenomena such as postvagal tachycardia[27, 28] or the biphasic response of initial HR reduction followed by acceleration during ICNS stimulation[29]. Large nerve fibers also tracked the crista terminalis, along which the impulse has been shown to preferentially propagate after exiting the SAN[30]. In addition to characterizing neuronal populations, our immunohistochemical and ultrastructural studies demonstrate the close association of glial cells with RAGP neurons and intraganglionic nerve processes. As higher level of serum S100B following AF ablation has been associated

with long-term treatment success, indicating that acute neural damage promoted freedom from arrhythmia recurrence[31], additional study of this cell population may prove critical in understanding ICNS control.

In the SAN region of multiple species, a dense meshwork of neurons has been characterized by immunohistochemical methods as predominantly cholinergic, although adrenergic-, nitrergic-, and peptidergic-positive fibers have also been identified in the rabbit and human[20, 21, 24, 32, 33]. Protein expression profiling indicates predominantly cholinergic neurons in the RAGP, but we describe the potential for expanded phenotypic diversity of RAGP neurons based on RNA analysis. For instance, neurons that expressed TH did not appear to be classically adrenergic, based on a lack of VMAT2 expression, and their function needs to be elucidated. Surprisingly, NPY, which is typically considered a cotransmitter for norepinephrine, was expressed in VAChT-positive cholinergic neurons in the RAGP and, conversely, in TH-positive fibers in the atrial myocardium. Peptidergic, putative sensory markers CGRP and SP were found in nerve fibers tracking through the ganglia but not the portion of the atrium we evaluated, which raises the question of how sensory information is transduced to RAGP neurons. Interestingly, transcripts of SP and its receptor are expressed within RAGP neurons but were not associated with significant protein expression on immunohistochemical study. While mechanical stimuli are thought to be transduced by the RAGP, the limbs of the Bainbridge reflex, the pathway by which atrial stretch induces HR increase, remains ill-defined[34, 35].

In addition to immunohistochemical study, prior work suggested the presence of adrenergic and cholinergic receptors in the GP based on response to neurochemicals; we are now able to provide a comprehensive library of genes expressed in intrinsic cardiac neurons[36, 37]. Using high-throughput gene expression profiling of RAGP neurons, we identified neural subpopulations, membrane receptors and ion channels that may be targeted by pharmacological agents upstream of the myocardium. In rat and canine intrinsic cardiac neurons, both nicotinic and muscarinic synaptic transmission has been studied[38, 39]. Here, we show that muscarinic receptors are expressed in the RAGP. Hence, when muscarinic antagonists such as atropine are applied, they may not simply affect muscarinic receptors at the atrial myocardium but also in the cardiac neurons. This may provide another explanation for seemingly paradoxical phenomena such as atropine-induce bradycardia[40, 41], as prior studies on the RAGP using atropine to mitigate cholinergic inputs to the myocardium may have inadvertently impacted RAGP neurophysiology[29, 42]. Genetic association studies that implicate muscarinic receptors in HR recovery in exercise or ion channels with sudden unexplained death in epilepsy are agnostic to tissue type[43, 44]. These variants may serve as markers for pathology in the nervous system rather than the myocardium. Similarly, the presence of HCN4 channels in cardiac neurons may suggest that the I_f blocker ivabradine may exert its action via I_h in the ICNS in addition to affecting the I_f in the SAN and warrants further study of how HCN4-positive cells in the SAN region influence its pacemaker function[45]. Delineation of neuronal subpopulations and molecular states by gene expression profiling suggests phenotypic diversity beyond what is ascertainable by immunohistochemistry or the application of pharmacological agents[46]. Characterizing the plasticity of RAGP arising due to dynamic shifts in these neuronal states may elucidate

molecular mechanisms driving pathophysiological response in heart disease to inform novel neuromodulatory interventions.

The present study further advances our knowledge of the functional innervation of the cardiac conduction system and working myocardium. VNS causes a shift in the pacemaker site and activation pattern within the SAN region[47–49]. Following the initial description that stimulation at an intercaval region of the RA conveys vagal input to the SAN[4], electrical stimulation of the RAGP fat pad was shown to reduce HR in dogs and humans[6, 50]. McGuirt et al.[51] showed that while ablation of the RAGP abolishes response to cervical bilateral VNS, VNS was still able to reduce the response to sympathetic stimulation, indicating that RAGP ablation eliminated direct, but not indirect, parasympathetic control of the SAN. This highlights the complex interplay between the cardiac GPs and higher levels of the cardiac neuraxis rather than cardiac GPs acting as relay stations[3]. A laterality has been ascribed to both vagal and sympathetic inputs to the SAN wherein the right vagus and stellate ganglion influence the SAN, the left vagus predominantly impacts the AVN and the left stellate affects LV inotropy[52, 53], although one study showed left vagal inputs via the RAGP[54]. We demonstrated that RAGP ablation impacts bilateral vagal inputs as well as the effect of the right vagus nerve on the AVN. This builds on a prior study in guinea pig that demonstrated a nerve tract extending from SAN, inferior to the ostium of the coronary sinus and toward the posterior aspect of the AVN, although this has been debated[32, 55]. Furthermore, as RAGP ablation also impacted LV contractility, our findings continue to challenge the notion that the GPs can be specifically targeted to independently influence SAN or AVN function, as proposed in animal models and human studies[56–58]. Although ablation of the region did not significantly impact SGS-induced tachycardia, neurons within the right stellate ganglia were identified after retrograde labeling which is consistent with right SGS-induced increases in SAN rate. Adjunctive ablation of the posterior atrial GP, which is located between the SVC and aorta, may have abolished SGS-induced tachycardia, as murine and canine models have suggested TH-positive fibers course via the medial aspect of the SVC to the SAN[59, 60]. As some cardiothoracic surgeons are exploring SAN denervation for SAN ablation for inappropriate sinus tachycardia, these findings suggest that the region of the RAGP-SAN should be spared[61].

We showed that RAGP stimulation typically induces reductions in atrial rate, but we also demonstrated changes in AVN conduction and induction of AF. Interestingly, bradycardia was easier to induce with decentralization following bilateral cervical vagotomies and vagosympathetic trunk debranching (ie bilateral stellate ganglionectomy). In the setting of vagotomies only, RAGP stimulation variably induced a mild bradycardia, while decentralization resulted in profound sinus bradycardia with ventricular asystole or AF. This suggests central input impacting the threshold to electrical stimulation and contrasts with prior studies where decentralization reduces response to pharmacological stimulation[36, 62]. Clinically, high-frequency stimulation using an endovascular approach to elicit a vagal response can be challenging, which is why some clinical trials have espoused an anatomic-guided approach to GP ablation[57, 58, 63]. Here, we show that central input to the ICNS tamps down the ability to induce a response to high-frequency stimulation. We further demonstrate this in our human atrial wedge preparation, a ‘decentralized’ state, in which we elicited a response with high-frequency stimulation. The response was tachycardic rather than

bradycardic and may have been due to increased frequency of stimulation, as we noted an increase in HR with up-titration of frequency in our porcine model (Figure XIA in the Data Supplement) and as a prior study in dogs in which GPs were stimulated at 200 Hz demonstrated ectopy followed by AF with uptitration of stimulation amplitude[64]. Alternatively, electrical stimulation may be impacting adrenergic fibers of passage *en passant* to the SAN. For example, studies in humans (ie in the absence of decentralization) suggested that RAGP stimulation affects the SAN without atrial-His prolongation[6, 65], while other canine studies describe bradycardia, tachycardia, atrial-His prolongation and AF induced by RAGP stimulation[56, 66, 67]. This further highlights the difficulty with specifically targeting only RAGP neurons as opposed to nerve tracts. However, given anatomy-guided identification and ablation of this region in patients, this is a clinically relevant approach. While intramural autonomic nerves in the vicinity of the SAN have been stimulated in an atrial wedge preparation in dog and rabbit to elicit a change in atrial rate, to our knowledge, this is the first description of how the RAGP exerts control over the pacemaker site[68, 69]. Importantly, clinical studies evaluating RAGP ablation for sinus node dysfunction have not reported sinus node electrograms to demonstrates effects on the sinus node itself[70].

The development of therapeutics that target the cardiac autonomic nervous system could provide an effective strategy for treating arrhythmias. However, as outlined by the present study, neuromodulatory therapies that target the RAGP to affect the SAN may result in off-target effects. In the AFACT study, in which patients were randomized to AF ablation with or without GP ablation, 5% of patients required pacemaker implantation, and 2-year follow-up did not show a reduction in AF recurrence[10, 71]. Heterogeneity in targets for intervention across studies has yielded variable results, and the approach of ablating GPs does not selectively target neurons, as afferent, efferent and local circuit neurons are likely impacted[9, 72]. Inappropriate sinus tachycardia has emerged as a consequence of disrupting parasympathetic fibers to the SAN, although SAN denervation has also been applied to cases of inappropriate sinus tachycardia[61, 73]. In studies of GP ablation for sinus bradycardia and syncope, radiofrequency ablation of the RAGP resulted in increased HRs and a 95% reduction in syncope, respectively, but the long-term consequences of such cardioneuroablation are, as yet, unclear[57, 58]. Phenotyping of neurons within the RAGP may allow for improved precision in targeting neuronal subpopulations with the goal of addressing specific aspects of cardiac control. One could speculate however that the redundancy of a distributed network of GPs maintains cardiac homeostasis.

Targeting cardiac neuronal subpopulations has been explored in preclinical studies. For instance, TRPV1 (transient receptor potential vanilloid 1)-expressing cardiac afferent neurons have been ablated using resinferatoxin, a ultrapotent analog of capsaicin, and shown to mitigate cardiac remodeling and autonomic dysfunction in a rat model of heart failure[74]. Epicardial application of resinferatoxin mitigated risk of post-myocardial infarction ventricular arrhythmia in a porcine model [75], and intrapericardial injection reduced AF inducibility in a canine model of apnea-induced AF [76]. Molecular phenotyping of the intrinsic cardiac nervous system holds the promise of expanding pharmacological therapies of clinical arrhythmia, which is further supported by novel surrogate markers characterized in human cardiovascular disease. Specifically, levels of circulating sympathetic cotransmitter NPY have been correlated to mortality risk in heart failure, post-myocardial infarction

ventricular arrhythmia and AF [77–79]. While elevations in NPY have been ascribed to release from sympathetic neurons, our finding of robust NPY expression in porcine intrinsic cardiac nervous system raises the possibility of cardiac neuronal release of the neurotransmitter. Given the recent interest in transcriptomics of the sinoatrial node[80–84], we hope that this study will complement this previously published work in further understanding pacemaking function, and the approach adopted for arrhythmias to help in the development of pharmacological treatments that target the intrinsic cardiac nervous system.

In short, this study affirmed the powerful cholinergic control of the RAGP over the SAN. For the first time, we provide a roadmap of RAGP gene and protein expression profiles and functional assays of RAGP effects on the SAN and whole heart. The work characterizes the RAGP as an integrative neural structure as opposed to a relay station within the distributed network of the ICNS. We set forth a foundation upon which further exploration of how the diverse neural population influences cardiac physiology and disease. This approach provides a template that may be adopted for defining other components of the ICNS to identify therapeutic targets within the autonomic nervous system to ameliorate cardiovascular disease.

Data Supplement

Refer to Web version on PubMed Central for supplementary material.

ACKNOWLEDGEMENTS

We dedicate this article to the esteemed J. Andrew Armour, MD, PhD, a pioneer in the study of the mammalian ICNS.[2, 3] We thank Sarah Hiyari, PhD, and Amiksha S. Gandhi, MS, for their contributions to the tissue clearing of porcine and human specimens, respectively, and Toru Adachi, MD, PhD; Taro Temma, MD, PhD; and Christopher Chan, BS, for their assistance with the porcine experiments. We extend special thanks to Warwick Peacock, MD; Michael C. Fishbein, MD; and the UCLA Donated Body Program for assistance with autopsy studies. We are also appreciative of the assistance of the UCLA Translational Pathology Core Laboratory for histological studies, California Nanosystems Institute for microCT imaging and the UCLA Broad Stem Cell Research Center Microscopy Core for imaging analysis. We thank James Weiss, MD; Noel Boyle, MD, PhD; and Olujimi Ajijola, MD, PhD, for their comments on the article. We are grateful to the NIH administrators Felicia Qashu, PhD, and Tyler Best, PhD, for their leadership in overseeing the NIH Common Fund's SPARC program.

SOURCES OF FUNDING

Funding for this work was provided by the NIH through the Common Fund's SPARC program, Grants OT2 OD023848 (PI: K.S.) and OT2 OD026585 (PI: L.A.H.); NHLBI Grants U01 EB025138 (PI: J.L.A. and K.S.) and U01 HL133360 (PI: J.S.S. and R.V.); and NHLBI Postdoctoral Fellowships T32 HL007895 (trainee: P.H.) and F32 HL152609 (PI: P.H.). Additional support for this work was provided by the Gordon Family Research Fund. P.H. is a fellow in the UCLA Specialty Training and Advanced Research (STAR) program.

Nonstandard Abbreviations and Acronyms:

AF	atrial fibrillation
AFACT	Atrial Fibrillation Ablation and Autonomic Modulation via Thoracoscopic Surgery
AVN	atrioventricular node
CGRP	calcitonin gene-related peptide

GP	ganglionated plexus
HCN4	hyperpolarization-activated cyclic nucleotide-gated channel 4
HR	heart rate
ICNS	Intrinsic cardiac nervous system
LV	left ventricle
MAP2	microtubule-associated protein 2
nNOS	neuronal nitric oxide synthase
NPY	neuropeptide Y
PGP9.5	protein gene product 9.5
RA	right atrium
RAGP	right atrial ganglionated plexus
SAN	sinoatrial node
SP	substance P
TH	tyrosine hydroxylase
TRPV1	transient receptor potential vanilloid 1
VAChT	vesicular acetylcholine transporter
VMAT2	vesicular monamine transporter 2
VNS	vagal nerve stimulation

REFERENCES

1. Shivkumar K, Ajijola OA, Anand I, Armour JA, Chen PS, Esler M, De Ferrari GM, Fishbein MC, Goldberger JJ, Harper RM, Joyner MJ, Khalsa SS, Kumar R, Lane R, Mahajan A, Po S, Schwartz PJ, Somers VK, Valderrabano M, Vaseghi M and Zipes DP. Clinical neurocardiology defining the value of neuroscience-based cardiovascular therapeutics. J Physiol. 2016;594:3911–54. [PubMed: 27114333]
2. Armour JA, Murphy DA, Yuan BX, MacDonald S and Hopkins DA. Gross and microscopic anatomy of the human intrinsic cardiac nervous system. The Anatomical Record: An Official Publication of the American Association of Anatomists. 1997;247:289–298.
3. Armour JA. Potential clinical relevance of the ‘little brain’on the mammalian heart. Experimental physiology. 2008;93:165–176. [PubMed: 17981929]
4. Lazzara R, Scherlag BJ, Robinson MJ and Samet P. Selective in situ parasympathetic control of the canine sinoatrial and atrioventricular nodes. Circulation Research. 1973;32:393–401. [PubMed: 4691345]
5. Ardell JL and Randall WC. Selective vagal innervation of sinoatrial and atrioventricular nodes in canine heart. American Journal of Physiology-Heart and Circulatory Physiology. 1986;251:H764–H773.

6. Carlson MD, Geha AS, Hsu J, Martin PJ, Levy MN, Jacobs G and Waldo AL. Selective stimulation of parasympathetic nerve fibers to the human sinoatrial node. Circulation. 1992;85:1311–1317. [PubMed: 1555275]
7. Wake E and Brack K. Characterization of the intrinsic cardiac nervous system. Autonomic Neuroscience. 2016;199:3–16. [PubMed: 27568996]
8. Randall DC, Brown DR, McGuirt AS, Thompson GW, Armour JA and Ardell JL. Interactions within the intrinsic cardiac nervous system contribute to chronotropic regulation. American Journal of Physiology-Regulatory, Integrative and Comparative Physiology. 2003;285:R1066–R1075.
9. Romanov A, Pokushalov E, Ponomarev D, Bayramova S, Shabanov V, Losik D, Stenin I, Elesin D, Mikheenko I and Strelnikov A. Long-term suppression of atrial fibrillation by botulinum toxin injection into epicardial fat pads in patients undergoing cardiac surgery: three-year follow-up of a randomized study. Heart Rhythm. 2019;16:172–177. [PubMed: 30414841]
10. Berger WR, Neefs J, van den Berg NW, Krul SP, van Praag EM, Piersma FR, de Jong JS, van Boven W-JP, Driessen AH and de Groot JR. Additional Ganglion Plexus Ablation During Thoracoscopic Surgical Ablation of Advanced Atrial Fibrillation: Intermediate Follow-Up of the AFACT Study. JACC: Clinical Electrophysiology. 2019;5:343–353. [PubMed: 30898238]
11. James TN, Zipes DP, Finegan RE, Eisele JW and Carter JE. Cardiac ganglionitis associated with sudden unexpected death. Annals of internal medicine. 1979;91:727–730. [PubMed: 496105]
12. Jungen C, Scherschel K, Eickholt C, Kuklik P, Klatt N, Bork N, Salzbrunn T, Alken F, Angendohr S and Klene C. Disruption of cardiac cholinergic neurons enhances susceptibility to ventricular arrhythmias. Nature communications. 2017;8:14155.
13. Rajendran PS, Challis RC, Fowlkes CC, Hanna P, Tompkins JD, Jordan MC, Hiyari S, Gabris-Weber BA, Greenbaum A and Chan KY. Identification of peripheral neural circuits that regulate heart rate using optogenetic and viral vector strategies. Nature communications. 2019;10:1–13.
14. Arora R, Waldmann M, Hopkins D and Armour J. Porcine intrinsic cardiac ganglia. The Anatomical Record Part A: Discoveries in Molecular, Cellular, and Evolutionary Biology: An Official Publication of the American Association of Anatomists. 2003;271:249–258.
15. Batulevicius D, Skripka V, Pauziene N and Pauza DH. Topography of the porcine epicardiac nerve plexus as revealed by histochemistry for acetylcholinesterase. Autonomic Neuroscience. 2008;138:64–75. [PubMed: 18063424]
16. Clauss S, Bleyer C, Schuettler D, Tomsits P, Renner S, Klymiuk N, Wakili R, Massberg S, Wolf E and Kääb S. Animal models of arrhythmia: classic electrophysiology to genetically modified large animals. Nature Reviews Cardiology. 2019;16:457–475. [PubMed: 30894679]
17. Schüttler D, Bapat A, Kääb S, Lee K, Tomsits P, Clauss S and Hucker WJ. Animal models of atrial fibrillation. Circulation Research. 2020;127:91–110. [PubMed: 32716814]
18. Renier N, Adams EL, Kirst C, Wu Z, Azevedo R, Kohl J, Autry AE, Kadiri L, Venkataraju KU and Zhou Y. Mapping of brain activity by automated volume analysis of immediate early genes. Cell. 2016;165:1789–1802. [PubMed: 27238021]
19. Achanta S, Gorky J, Leung C, Moss A, Robbins S, Eisenman L, Chen J, Tappan S, Heal M, Farahani N, Huffman T, England S, Cheng Z, Vadigepalli R and Schwaber JS. A Comprehensive Integrated Anatomical and Molecular Atlas of Rat Intrinsic Cardiac Nervous System. iScience. 2020:101140. [PubMed: 32460006]
20. Rysevaite K, Saburkina I, Pauziene N, Vaitkevicius R, Noujaim SF, Jalife J and Pauza DH. Immunohistochemical characterization of the intrinsic cardiac neural plexus in whole-mount mouse heart preparations. Heart Rhythm. 2011;8:731–738. [PubMed: 21232628]
21. Hoover D, Isaacs E, Jacques F, Hoard J, Page P and Armour J. Localization of multiple neurotransmitters in surgically derived specimens of human atrial ganglia. Neuroscience. 2009;164:1170–1179. [PubMed: 19747529]
22. Mick J, Wurster R, Duff M, Weber M, Randall W and Randall D. Epicardial sites for vagal mediation of sinoatrial function. American Journal of Physiology-Heart and Circulatory Physiology. 1992;262:H1401–H1406.
23. Jacobowitz D Histochemical studies of the relationship of chromaffin cells and adrenergic nerve fibers to the cardiac ganglia of several species. Journal of Pharmacology and Experimental Therapeutics. 1967;158:227–240.

24. Crick SJ, Wharton J, Sheppard MN, Royston D, Yacoub MH, Anderson RH and Polak JM. Innervation of the human cardiac conduction system. A quantitative immunohistochemical and histochemical study. Circulation. 1994;89:1697–1708. [PubMed: 7908612]
25. Pauza DH, Skripka V, Pauziene N and Stropus R. Anatomical study of the neural ganglionated plexus in the canine right atrium: implications for selective denervation and electrophysiology of the sinoatrial node in dog. The Anatomical Record: An Official Publication of the American Association of Anatomists. 1999;255:271–294.
26. Ai J, Epstein P, Gozal D, Yang B, Wurster R and Cheng Z. Morphology and topography of nucleus ambiguus projections to cardiac ganglia in rats and mice. Neuroscience. 2007;149:845–860. [PubMed: 17942236]
27. Copen DL, Cirillo DP and Vassalle M. Tachycardia following vagal stimulation. American Journal of Physiology-Legacy Content. 1968;215:696–703.
28. Vassalle M, Mandel WJ and Holder MS. Catecholamine stores under vagal control. American Journal of Physiology-Legacy Content. 1970;218:115–123.
29. Zarzoso M, Rysevaite K, Milstein ML, Calvo CJ, Kean AC, Atienza F, Pauza DH, Jalife J and Noujaim SF. Nerves projecting from the intrinsic cardiac ganglia of the pulmonary veins modulate sinoatrial node pacemaker function. Cardiovascular research. 2013;99:566–575. [PubMed: 23559611]
30. Opthof T, de Jonge B, Jongsma HJ and Bouman LN. Functional morphology of the pig sinoatrial node. Journal of molecular and cellular cardiology. 1987;19:1221–1236. [PubMed: 2832616]
31. Scherschel K, Hedenus K, Jungen C, Lemoine MD, Rübsamen N, Veldkamp MW, Klatt N, Lindner D, Westermann D and Casini S. Cardiac glial cells release neurotrophic S100B upon catheter-based treatment of atrial fibrillation. Science translational medicine. 2019;11.
32. Hoover DB, Ganote CE, Ferguson SM, Blakely RD and Parsons RL. Localization of cholinergic innervation in guinea pig heart by immunohistochemistry for high-affinity choline transporters. Cardiovascular research. 2004;62:112–121. [PubMed: 15023558]
33. Inokaitis H, Pauziene N, Rysevaite-Kyguoliene K and Pauza DH. Innervation of sinoatrial nodal cells in the rabbit. Annals of Anatomy-Anatomischer Anzeiger. 2016;205:113–121.
34. Bainbridge F The influence of venous filling upon the rate of the heart. The Journal of physiology. 1915;50:65–84. [PubMed: 16993330]
35. Thompson G, Collier K, Ardell J, Kember G and Armour J. Functional interdependence of neurons in a single canine intrinsic cardiac ganglionated plexus. The Journal of physiology. 2000;528:561–571. [PubMed: 11060132]
36. Armour J, Huang M and Smith F. Peptidergic modulation of in situ canine intrinsic cardiac neurons. Peptides. 1993;14:191–202. [PubMed: 8483797]
37. Xu Z-J and Adams DJ. Alpha-adrenergic modulation of ionic currents in cultured parasympathetic neurons from rat intracardiac ganglia. Journal of neurophysiology. 1993;69:1060–1070. [PubMed: 8098358]
38. Xi-Moy S, Randall W and Wurster R. Nicotinic and muscarinic synaptic transmission in canine intracardiac ganglion cells innervating the sinoatrial node. Journal of the autonomic nervous system. 1993;42:201–213. [PubMed: 8096229]
39. Beker F, Weber M, Fink RH and Adams DJ. Muscarinic and nicotinic ACh receptor activation differentially mobilize Ca2+ in rat intracardiac ganglion neurons. Journal of neurophysiology. 2003;90:1956–1964. [PubMed: 12761283]
40. Meyer E and De Sommers K. Possible mechanisms of anti-cholinergic drug-induced bradycardia. European journal of clinical pharmacology. 1988;35:503–506. [PubMed: 3234460]
41. Ikuta Y, Shimoda O and Kano T. Quantitative assessment of the autonomic nervous system activities during atropine-induced bradycardia by heart rate spectral analysis. Journal of the autonomic nervous system. 1995;52:71–76. [PubMed: 7782571]
42. Allen E, Coote JH, Grubb BD, Batten TF, Pauza DH, Ng GA and Brack KE. Electrophysiological effects of nicotinic and electrical stimulation of intrinsic cardiac ganglia in the absence of extrinsic autonomic nerves in the rabbit heart. Heart rhythm. 2018;15:1698–1707. [PubMed: 29800749]
43. Hautala AJ, Rankinen T, Kiviniemi AM, Makikallio TH, Huikuri HV, Bouchard C and Tulppo MP. Heart rate recovery after maximal exercise is associated with acetylcholine receptor M2 (CHRM2)

gene polymorphism. American Journal of Physiology-Heart and Circulatory Physiology. 2006;291:H459–H466. [PubMed: 16501017]

44. Friedman D, Kannan K, Faustin A, Shroff S, Thomas C, Heguy A, Serrano J, Snuderl M and Devinsky O. Cardiac arrhythmia and neuroexcitability gene variants in resected brain tissue from patients with sudden unexpected death in epilepsy (SUDEP). NPJ genomic medicine. 2018;3:1–8. [PubMed: 29354286]
45. Bychkov R, Juhaszova M, Tsutsui K, Coletta C, Stern MD, Maltsev VA and Lakatta EG. Synchronized Cardiac Impulses Emerge From Heterogeneous Local Calcium Signals Within and Among Cells of Pacemaker Tissue. JACC: Clinical Electrophysiology. 2020;6:907–931. [PubMed: 32819526]
46. Moss A, Robbins S, Achanta S, Kuttippurathu L, Turick S, Nieves S, Hanna P, Smith EH, Hoover DB, Chen J, Cheng Z, Ardell JL, Shivkumar K, Schwaber JS and Vadigepalli R. A spatially-tracked single cell transcriptomics map of neuronal networks in the intrinsic cardiac nervous system. bioRxiv. 2020:2020.07.29.227090.
47. Meek W and Eyster J. The effect of vagal stimulation and of colling on the location of the pacemaker within the sino-auricular node. The American journal of physiology. 1914;34:368–383.
48. Bouman L, Gerlings E, Biersteker P and Bonke F. Pacemaker shift in the sino-atrial node during vagal stimulation. Pflügers Archiv. 1968;302:255–267. [PubMed: 5748559]
49. Goldberg JM. Intra-SA-nodal pacemaker shifts induced by autonomic nerve stimulation in the dog. American Journal of Physiology-Legacy Content. 1975;229:1116–1123.
50. Butler C, Smith F, Cardinal R, Murphy D, Hopkins D and Armour J. Cardiac responses to electrical stimulation of discrete loci in canine atrial and ventricular ganglionated plexi. American Journal of Physiology-Heart and Circulatory Physiology. 1990;259:H1365–H1373.
51. McGuirt AS, Schmacht DC and Ardell JL. Autonomic interactions for control of atrial rate are maintained after SA nodal parasympathectomy. The American journal of physiology. 1997;272:H2525–33. [PubMed: 9227527]
52. Ng GA, Brack KE and Coote JH. Effects of direct sympathetic and vagus nerve stimulation on the physiology of the whole heart-a novel model of isolated Langendorff perfused rabbit heart with intact dual autonomic innervation. Experimental physiology. 2001;86:319–329. [PubMed: 11471534]
53. Winter J, Tanko AS, Brack KE, Coote JH and Ng GA. Differential cardiac responses to unilateral sympathetic nerve stimulation in the isolated innervated rabbit heart. Autonomic Neuroscience. 2012;166:4–14. [PubMed: 21930436]
54. Hou Y, Scherlag BJ, Lin J, Zhang Y, Lu Z, Truong K, Patterson E, Lazzara R, Jackman WM and Po SS. Ganglionated plexi modulate extrinsic cardiac autonomic nerve input: effects on sinus rate, atrioventricular conduction, refractoriness, and inducibility of atrial fibrillation. Journal of the American College of Cardiology. 2007;50:61–68. [PubMed: 17601547]
55. Batulevicius D, Pauziene N and Pauza DH. Architecture and age-related analysis of the neuronal number of the guinea pig intrinsic cardiac nerve plexus. Annals of Anatomy-Anatomischer Anzeiger. 2005;187:225–243.
56. Furukawa Y, Wallick DW, Martin PJ and Levy M. Chronotropic and dromotropic responses to stimulation of intracardiac sympathetic nerves to sinoatrial or atrioventricular nodal region in anesthetized dogs. Circulation research. 1990;66:1391–1399. [PubMed: 2335032]
57. Qin M, Zhang Y, Liu X, Jiang W-F, Wu S-H and Po S. Atrial ganglionated plexus modification: a novel approach to treat symptomatic sinus bradycardia. JACC: Clinical Electrophysiology. 2017;3:950–959. [PubMed: 29759719]
58. Debruyne P, Rossenbacker T, Collienne C, Roosen J, Ector B, Janssens L, Charlier F, Vankelecom B, Dewilde W and Wijns W. Unifocal right-sided ablation treatment for neurally mediated syncope and functional sinus node dysfunction under computed tomographic guidance. Circulation: Arrhythmia and Electrophysiology. 2018;11:e006604. [PubMed: 30354289]
59. Randall DC, Brown DR, Li S-G, Olmstead ME, Kilgore JM, Sprinkle AG, Randall WC and Ardell JL. Ablation of posterior atrial ganglionated plexus potentiates sympathetic tachycardia to behavioral stress. American Journal of Physiology-Regulatory, Integrative and Comparative Physiology. 1998;275:R779–R787.

60. Gray AL, Johnson TA, Ardell JL and Massari VJ. Parasympathetic control of the heart. II. A novel interganglionic intrinsic cardiac circuit mediates neural control of heart rate. Journal of Applied Physiology. 2004;96:2273–2278. [PubMed: 14978001]
61. Khiabani AJ, Greenberg JW, Hansalia VH, Schuessler RB, Melby SJ and Damiano RJ Jr. Late Outcomes of Surgical Ablation for Inappropriate Sinus Tachycardia. The Annals of thoracic surgery. 2019;108:1162–1168. [PubMed: 31077661]
62. Yuan B-X, Ardell J, Hopkins D and Armour J. Differential cardiac responses induced by nicotine sensitive canine atrial and ventricular neurones. Cardiovascular research. 1993;27:760–769. [PubMed: 8348576]
63. Katritsis DG, Pokushalov E, Romanov A, Giazitzoglou E, Siontis GC, Po SS, Camm AJ and Ioannidis JP. Autonomic denervation added to pulmonary vein isolation for paroxysmal atrial fibrillation: a randomized clinical trial. Journal of the American College of Cardiology. 2013;62:2318–2325. [PubMed: 23973694]
64. Schauerte P, Scherlag BJ, Patterson E, Scherlag MA, Matsudaria K, Nakagawa H, Lazzara R and Jackman WM. Focal atrial fibrillation: experimental evidence for a pathophysiologic role of the autonomic nervous system. Journal of cardiovascular electrophysiology. 2001;12:592–599. [PubMed: 11386522]
65. Quan KJ, Lee JH, Geha AS, Biblo LA, VAN HARE GF, Mackall JA and Carlson MD. Characterization of sinoatrial parasympathetic innervation in humans. Journal of cardiovascular electrophysiology. 1999;10:1060–1065. [PubMed: 10466486]
66. Hou Y, Scherlag BJ, Lin J, Zhou J, Song J, Zhang Y, Patterson E, Lazzara R, Jackman WM and Po SS. Interactive atrial neural network: determining the connections between ganglionated plexi. Heart Rhythm. 2007;4:56–63. [PubMed: 17198991]
67. Cardinal R, Pagé P, Vermeulen M, Ardell JL and Armour JA. Spatially divergent cardiac responses to nicotinic stimulation of ganglionated plexus neurons in the canine heart. Autonomic Neuroscience. 2009;145:55–62. [PubMed: 19071069]
68. Furukawa Y and Levy MN. Temporal changes in he sympathetic-parasympathetic interactions that occur in the perfused canine atrium. Circulation research. 1984;55:835–841. [PubMed: 6499139]
69. Fedorov VV, Hucker WJ, Dobrzynski H, Rosenshtraukh LV and Efimov IR. Postganglionic nerve stimulation induces temporal inhibition of excitability in rabbit sinoatrial node. American Journal of Physiology-Heart and Circulatory Physiology. 2006;291:H612–H623. [PubMed: 16565321]
70. Hu F, Zheng L, Liang E, Ding L, Wu L, Chen G, Fan X and Yao Y. Right anterior ganglionated plexus: The primary target of cardioneuroablation? Heart rhythm. 2019;16:1545–1551. [PubMed: 31330187]
71. Driessen AH, Berger WR, Krul SP, van den Berg NW, Neefs J, Piersma FR, Yin DRCP, de Jong JS, van Boven WP and de Groot JR. Ganglion plexus ablation in advanced atrial fibrillation: the AFACT study. Journal of the American College of Cardiology. 2016;68:1155–1165. [PubMed: 27609676]
72. Waldron NH, Cooter M, Haney JC, Schroder JN, Gaca JG, Lin SS, Sigurdsson MI, Fudim M, Podgoreanu MV and Stafford-Smith M. Temporary autonomic modulation with botulinum toxin type A to reduce atrial fibrillation after cardiac surgery. Heart Rhythm. 2019;16:178–184. [PubMed: 30414840]
73. Friedman PL, Stevenson WG and Kocovic DZ. Autonomic dysfunction after catheter ablation. Journal of cardiovascular electrophysiology. 1996;7:450–459. [PubMed: 8722590]
74. Wang H-J, Wang W, Cornish KG, Rozanski GJ and Zucker IH. Cardiac sympathetic afferent denervation attenuates cardiac remodeling and improves cardiovascular dysfunction in rats with heart failure. Hypertension. 2014:HYPERTENSIONAHA. 114.03699.
75. Yoshie K, Rajendran PS, Massoud L, Mistry J, Swid MA, Wu X, Sallam T, Zhang R, Goldhaber JI and Salavatian S. Cardiac TRPV1 afferent signaling promotes arrhythmogenic ventricular remodeling after myocardial infarction. JCI insight. 2020;5.
76. Tavares L, Rodríguez-Mañero M, Kreidieh B, Ibarra-Cortez SH, Chen J, Wang S, Markovits J, Barrios R and Valderrábano M. Cardiac Afferent Denervation Abolishes Ganglionated Plexi and Sympathetic Responses to Apnea: Implications for Atrial Fibrillation. Circulation: Arrhythmia and Electrophysiology. 2019;12:e006942. [PubMed: 31164004]

77. Kalla M, Hao G, Tapoulal N, Tomek J, Liu K, Woodward L, Study' OAMI, Dall'Armellina E, Banning AP and Choudhury RP. The cardiac sympathetic co-transmitter neuropeptide Y is pro-arrhythmic following ST-elevation myocardial infarction despite beta-blockade. European heart journal. 2020;41:2168–2179. [PubMed: 31834357]

78. Ajijola OA, Chatterjee NA, Gonzales MJ, Gornbein J, Liu K, Li D, Paterson DJ, Shivkumar K, Singh JP and Herring N. Coronary sinus neuropeptide Y levels and adverse outcomes in patients with stable chronic heart failure. Jama Cardiology. 2020;5:318–325. [PubMed: 31876927]

79. Stavrakis S, Morris L, Takashima AD, Elkholey K, Van Wagoner DR and Ajijola OA. Circulating Neuropeptide Y as a Biomarker for Neuromodulation in Atrial Fibrillation. Clinical Electrophysiology. 2020;6:1575–1576. [PubMed: 33213819]

80. Vedantham V, Galang G, Evangelista M, Deo RC and Srivastava D. RNA sequencing of mouse sinoatrial node reveals an upstream regulatory role for Islet-1 in cardiac pacemaker cells. Circulation research. 2015;116:797–803. [PubMed: 25623957]

81. Linscheid N, Logantha SJR, Poulsen PC, Zhang S, Schrölkamp M, Egerod KL, Thompson JJ, Kitmitto A, Galli G and Humphries MJ. Quantitative proteomics and single-nucleus transcriptomics of the sinus node elucidates the foundation of cardiac pacemaking. Nature communications. 2019;10:1–19.

82. van Eif VW, Stefanovic S, van Duijvenboden K, Bakker M, Wakker V, de Gier-de Vries C, Zaffran S, Verkerk AO, Boukens BJ and Christoffels VM. Transcriptome analysis of mouse and human sinoatrial node cells reveals a conserved genetic program. Development. 2019;146.

83. Goodyer WR, Beyersdorf BM, Paik DT, Tian L, Li G, Buikema JW, Chirikian O, Choi S, Venkatraman S and Adams EL. Transcriptomic profiling of the developing cardiac conduction system at single-cell resolution. Circulation research. 2019;125:379–397. [PubMed: 31284824]

84. Galang G, Mandla R, Ruan H, Jung C, Sinha T, Stone NR, Wu RS, Mannion BJ, Allu PK and Chang K. ATAC-seq reveals an Isl1 enhancer that regulates sinoatrial node development and function. Circulation Research. 2020;127:1502–1518. [PubMed: 33044128]

85. Munro B Manual of histologic staining methods of the Armed Forces Institute of Pathology. Pathology. 1971;3:249.

86. Kaestner CL, Smith EH, Peirce SG and Hoover DB. Immunohistochemical analysis of the mouse celiac ganglion: An integrative relay station of the peripheral nervous system. Journal of Comparative Neurology. 2019;527:2742–2760.

87. Untergasser A, Cutcutache I, Koressaar T, Ye J, Faircloth BC, Remm M and Rozen SG. Primer3—new capabilities and interfaces. Nucleic acids research. 2012;40:e115–e115. [PubMed: 22730293]

88. Ye J, Coulouris G, Zaretskaya I, Cutcutache I, Rozen S and Madden TL. Primer-BLAST: a tool to design target-specific primers for polymerase chain reaction. BMC bioinformatics. 2012;13:134. [PubMed: 22708584]

89. Tompkins JD, Clason TA, Buttolph TR, Girard BM, Linden AK, Hardwick JC, Merriam LA, May V and Parsons RL. Src family kinase inhibitors blunt PACAP-induced PAC1 receptor endocytosis, phosphorylation of ERK, and the increase in cardiac neuron excitability. Am J Physiol Cell Physiol. 2018;314:C233–C241. [PubMed: 29141923]

90. Haws CW and Lux RL. Correlation between in vivo transmembrane action potential durations and activation-recovery intervals from electrograms. Effects of interventions that alter repolarization time. Circulation. 1990;81:281–288. [PubMed: 2297832]

NOVELTY AND SIGNIFICANCE

What Is Known?

- The sinoatrial node (SAN), the biologic pacemaker of the heart, is under neural control.
- Parasympathetic and sympathetic influences over the SAN have been previously evaluated, but there is a paucity of data regarding nerve populations in the heart that affect pacemaking.

What New Information Does This Article Contribute?

- A comprehensive atlas of the connections between neurons found in the heart in the right atrial ganglionated plexus (RAGP) and the SAN has been developed.
- Gene and protein expression analysis of RAGP demonstrates a rich diversity of neurons and expands upon just parasympathetic and sympathetic profiling in the past.
- These neurons connect to other neurons and cardiac muscle to control sinoatrial rate and location of earliest cardiac electrical activity at the pacemaker as well as atrioventricular conduction and left ventricular contractile function.

Cardiac function is under neural control, and interventions targeting cardiac neuronal populations on the surface of the heart for cardiovascular disease have shown mixed results. Understanding neural circuits that regulate cardiac function is critical to characterize their role in cardiovascular disease states. Here, we showcase a multiscale approach to provide in-depth phenotyping and functional assays of neurons at the RAGP that regulate pacemaking activity of the porcine and human SAN. We demonstrate that these neurons clustered in ganglia are interconnected and, while predominantly cholinergic, exhibit a diverse gene and protein expression profile. Ablation of the RAGP impacted not only SAN function but also atrioventricular nodal (AVN) function and left ventricular contractility. Furthermore, electrical stimulation of the RAGP influenced the pacemaking activity and site in the SAN. We envision that this approach may serve as a framework for future study of how cardiac neurons regulate distinct regions of the heart.

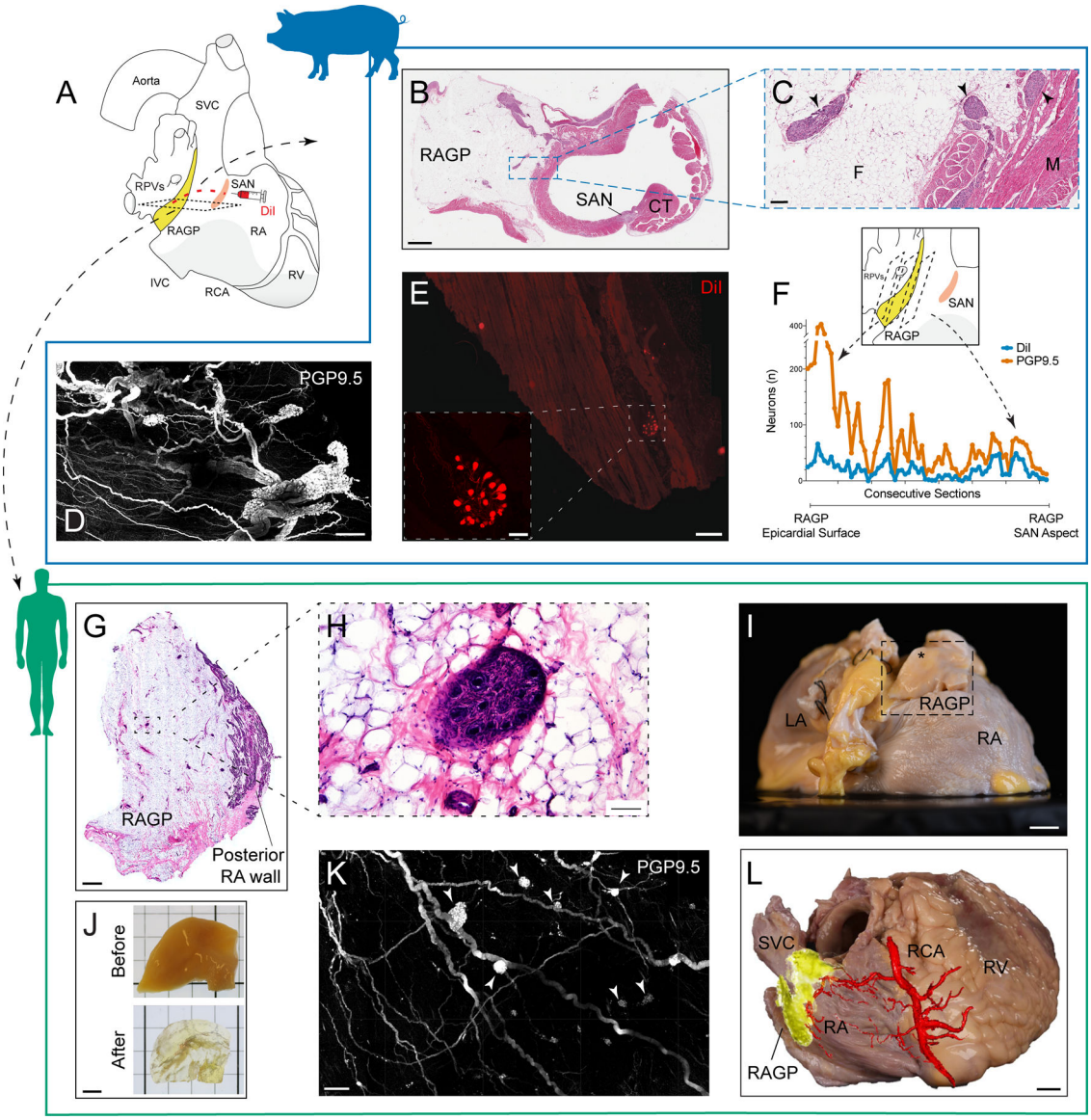

Figure 1. Neuroanatomy and vascular supply of the porcine and human right atrial ganglionated plexus (RAGP) in relation to the sinoatrial node (SAN).

A, Schematic of human heart demonstrating proximity of RAGP to SAN. DiI was injected into the porcine SAN followed by tissue harvest of RAGP 3 wk later. **B**, Hematoxylin and eosin (H&E) staining of porcine RAGP-SAN region in a male pig imaged at 20×. **C**, Ganglia (arrowheads) suspended in adipose tissue as well as at fat-RA muscle interface at higher magnification. **D**, Maximum intensity projection (MIP) of modified immunolabeling-enabled 3-dimensional imaging of solvent-cleared organs (iDISCO+)-cleared RAGP from a male pig illustrating cluster of interconnected ganglia with PGP9.5 (protein gene product 9.5; white). **E**, Example of DiI-labeled neurons and nerve fibers in a ganglion in the RAGP. Higher magnification of DiI-labeled ganglion is shown (inset). **F**, Quantification of DiI- and PGP9.5-positive and total neurons from a female pig. Eight representative sets of sections were collected from each RAGP in this study, and this data was obtained from one set that spanned the entire RAGP (1.8 cm). **G**, H&E staining of human RAGP fat pad at the

posterior RA wall. **H**, Ganglion suspended in fat at higher magnification. **I**, Right posterior oblique view of gross anatomy of a second human RAGP dissected (inset) for tissue clearing. Dissection contained epicardial fat (*) with adjacent muscle. **J**, Portion of human RAGP before and after iDISCO+ tissue clearing. **K**, MIP of iDISCO+-cleared portion of human RAGP demonstrating clusters of interconnected ganglia (arrowheads) with PGP 9.5 (white). **L**, Photograph of right posterior oblique view of a third human heart with overlay of microCT image of contrast-media-injected right coronary artery showing RAGP is supplied by the sinoatrial nodal artery. Scale bars are 2 mm (**B** and **G**), 200 μm (**C**), 500 μm (**D**, **K**, and **E**), 100 μm (**E inset and H**), 1 cm (**I** and **L**), and 5 mm (**J**). CT indicates crista terminalis; F, fat; LA, left atrium; and M, muscle.

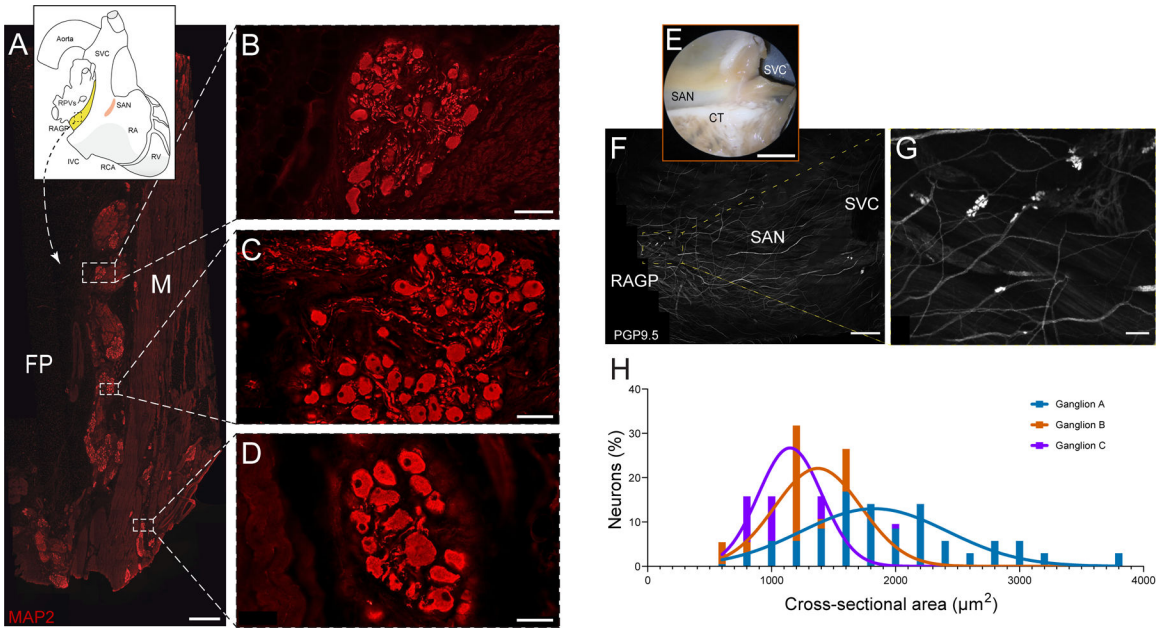

Figure 2. Immunohistochemical characterization of distribution and morphology of ganglia in the right atrial ganglionated plexus (RAGP) fat pad.

A, Photomontage of section that was immunostained for the pan-neuronal marker MAP2 (microtubule-associated protein 2; red). This figure was created from 165 overlapping 10× fluorescence images. **B–D**, Three ganglia shown at higher magnification. Most ganglia occur near the interface between the fat pad (FP) and atrial muscle (M), although some occur between muscle bundles (**D**). **E**, Photograph of sinoatrial node (SAN) region of RAGP-SAN tissue from a male pig that underwent whole-mount staining for PGP9.5 (protein gene product 9.5, white; **F**). **G**, Examples of 3 ganglia identified in F that underwent quantification of cross-sectional area (**H**). Frequency histograms were fitted with a gaussian plot to show the distribution of cell sizes for each ganglion. Five porcine RAGPs (3 males and 2 females) were evaluated in the immunohistochemical studies. Scale bars are 1 mm (**A**), 50 μm (**B and D**), 100 μm (**C**), 1 cm (**E**), 2.5 mm (**F**), and 200 μm (**G**).

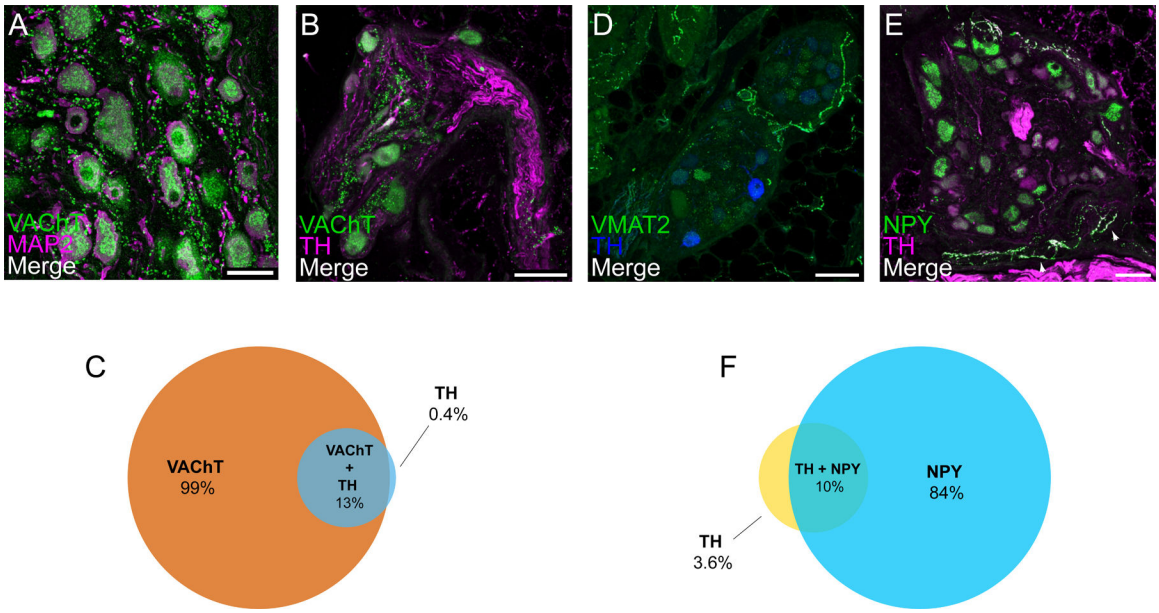

Figure 3. Ganglia in the right atrial ganglionated plexus (RAGP) contain cholinergic neurons and receive cholinergic input.

A, Confocal image of a ganglion double labeled for cholinergic marker VAChT (vesicular acetylcholine transporter) and for MAP2 (microtubule-associated protein 2). VAChT appears as granular staining of neuronal cell bodies and varicose staining in the neuropil. Neuronal cell bodies and processes are more fully delineated by MAP2 staining. Colocalization of VAChT and MAP2 cell bodies and the close association of VAChT-positive varicosities to cell bodies and nerve processes are shown. **B**, Confocal image of a ganglion double labeled for VAChT and for noradrenergic marker tyrosine hydroxylase (TH) indicate some neurons that contain VAChT and TH. Venn diagram illustrates proportion of VAChT-positive, TH-positive, and both VAChT- and THpositive neurons (**C**). **D**, A few RAGP neurons stain for TH but usually lack the essential noradrenergic marker VMAT2 (vesicular monoamine transporter 2), although positive staining for VMAT2 does occur in nerve fibers. Confocal image of a ganglion double labeled for NPY (neuropeptide Y) and TH (**E**) illustrate that many neurons show moderate to intense, granular labeling for NPY, but the same neurons lack TH. In contrast, NPY and TH colocalized in some nerve fibers. Nerve fibers labeled for NPY and TH (arrowheads) are sparse within ganglia and not in close apposition to ganglionic neurons. Venn diagram illustrates proportion of NPY-positive, TH-positive, and both NPY- and TH-positive neurons (**F**). Each value is based on analysis of confocal images from at least 8 microscopic fields in porcine RAGP (n=4; 2 males and 2 females). Scale bars are 50 μm (**A**) and 100 μm (**B, D, and E**).

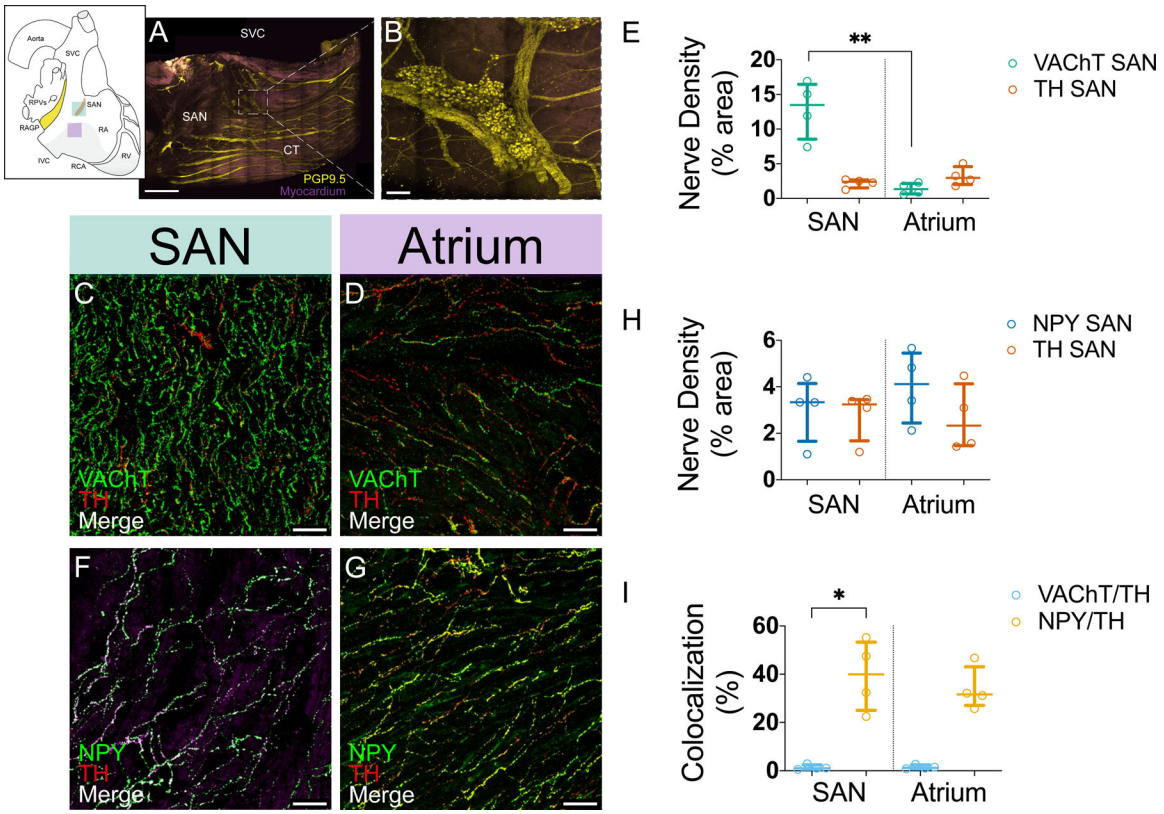

Figure 4. Cholinergic and noradrenergic nerves supply the sinoatrial node (SAN) and atrial myocardium at different densities.

A, Maximum intensity projection of modified immunolabeling-enabled 3-dimensional imaging of solvent-cleared organs (iDISCO+)-cleared female porcine SAN illustrating ganglia and network of nerves (yellow). Purple: muscle autofluorescence. **B**, Ganglia found in SAN region at higher magnification. Sections of SAN (**C**) and right atrial (RA) myocardium (**D**) were double labeled for VAChT (vesicular acetylcholine transporter) and TH. Confocal images from these sections show that cholinergic nerves are more abundant than noradrenergic nerves in the SAN (**C**) and that both nerve types have similar density in atrial myocardium (**D**). VAChT and TH are not colocalized. **E**, Density of cholinergic and noradrenergic nerves in the SAN and RA myocardium. Sections of SAN (**F**) and RA myocardium (**G**) were double labeled for NPY (neuropeptide Y) and TH. Confocal images from these sections show that staining for NPY and TH labeled the same population of nerves in both regions and have extensive colocalization. **H**, Density of NPY-positive and TH-positive nerves in the SAN and RA myocardium. Sections were double labeled for these markers. **I**, TH is not colocalized with VAChT but is colocalized with NPY in the SAN and RA. Each value (median [interquartile range]) is based on analysis of confocal images from at least 5 microscopic fields from 4 right atrial ganglionated plexuses (RAGPs; 2M/2F). Comparisons were made using Kruskal-Wallis and Dunn multiple comparisons tests. *Adjusted P≤0.05, **adjusted P≤0.01. Scale bars are 2 mm (**A**), 200 μm (**B**), and 50 μm (**C–G**).

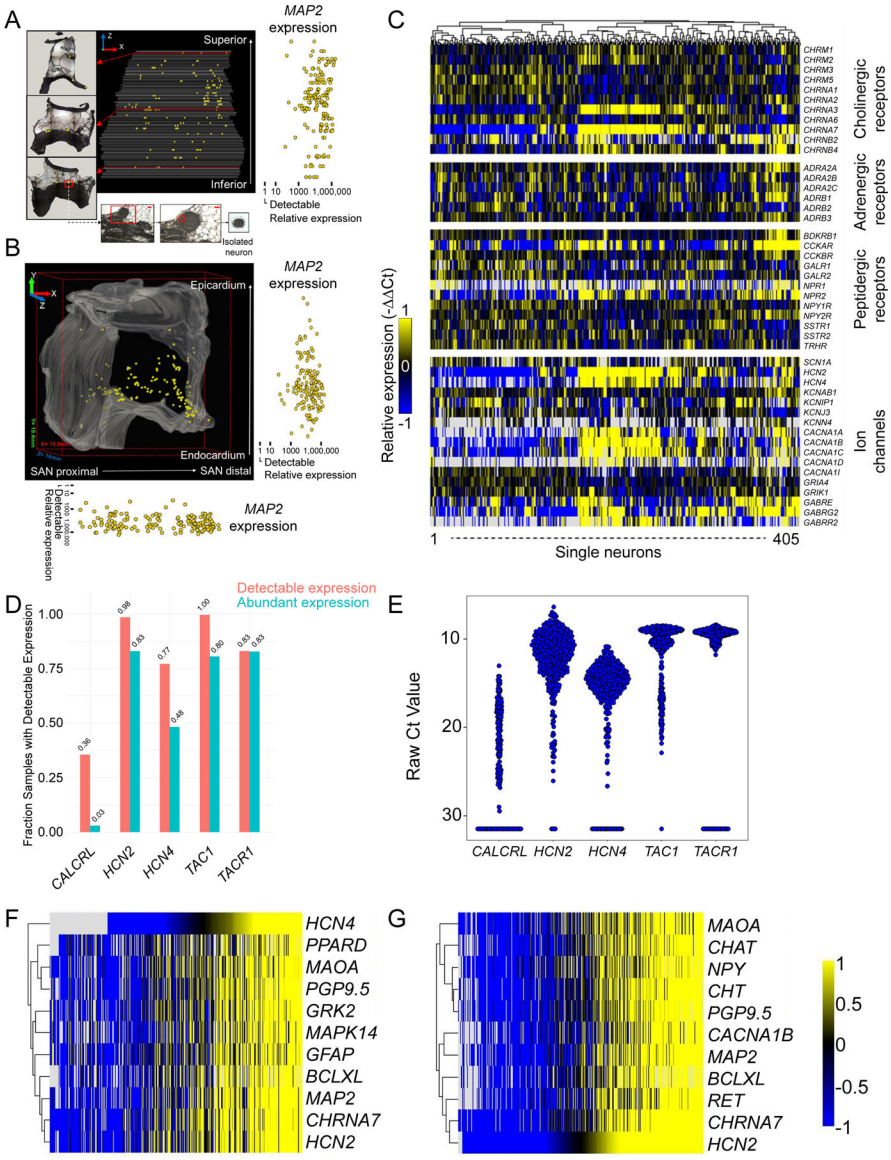

Figure 5. Diverse gene expression profile of porcine right atrial ganglionated plexus (RAGP) neurons.

Projections of neurons isolated within the RAGP and their relative expression of pan-neuronal marker *MAP2* (microtubule-associated protein 2) in the XZ (**A**) and XY (**B**) planes compared with the minimum level of detection. **C**, Heat map demonstrating diverse profile of neurotransmitters, adrenergic, cholinergic, and peptidergic receptors and ion channels in RAGP neurons. **D**, A significant proportion of RAGP neurons exhibit high gene expression of *HCN2* and *HCN4*. High expression of *TAC1* and *TACR1* genes, which are sensory markers, was identified. A smaller proportion expressed the gene encoding the receptor for CGRP (*CALCRL*). The range of expression of these genes is shown in **E**. The top 10 genes with correlated expression to *HCN2* (Pearson correlation coefficient >0.82; (**F**) and *HCN4* (Pearson correlation coefficient >0.67; (**G**) are shown. Note that high coexpression of pan-neuronal markers, neurotransmitters, nicotinic cholinergic receptor, and downstream signaling molecules such as G-protein–coupled receptor kinase 2 (*GRK2*).

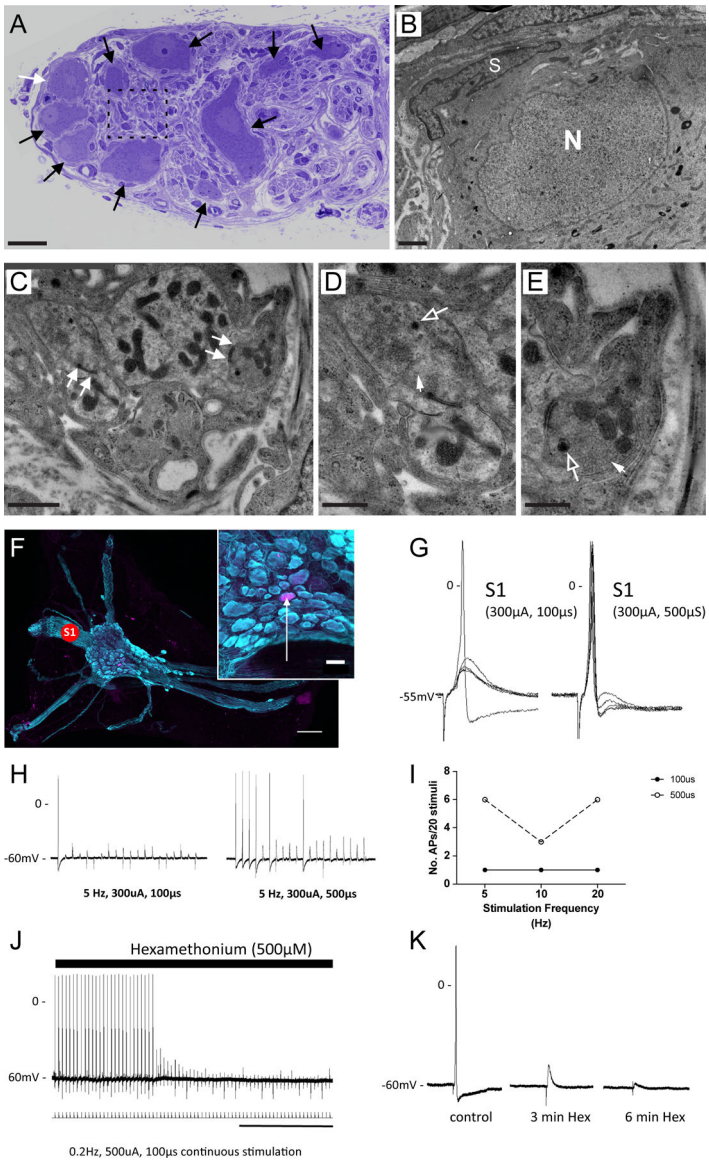

Figure 6. Convergence of cholinergic synaptic input at the right atrial ganglionated plexus (RAGP).

A, Light microscopy image shows toluidine blue labeled RAGP neurons (arrows). **B**, Transmission electron microscopic (TEM) image of neuron highlighted by white arrow in A. Note cell body nucleus (N) and satellite cell (S). No synaptic boutons are detected surrounding the cell body. **C-E**, TEM of synaptic boutons in contact with dendritic profiles in the porcine RAGP (detected in regions highlighted by dashed line **A**). Note synaptic specializations in the form of active zones (arrows in **C**). The synaptic boutons contain clear rounded vesicles (closed arrows) and a few dense-core vesicles (open arrows). Each synaptic bouton-dendrite complex is in close apposition with surrounding satellite glial processes. **F**, Representative ganglion within the RAGP. Note the many nerve bundles emanating from the ganglion. Concentric bipolar stimulating electrodes were placed on interganglionic nerves (S1) to elicit synaptic responses. Inset shows location of neuron (arrow) labeled with neurobiotin from the recording electrode. **G**, Representative membrane potential responses

recorded from the cell in F to stimulation at S1 are shown. There were no failures. Increasing stimulus current duration from 100 to 500 μs increased the probability of generating an action potential due to the larger evoked excitatory postsynaptic potential (EPSP), demonstrating a convergence of inputs. **H**, Synaptic efficacy was evaluated during continuous trains of presynaptic stimulation at the two pulse widths. Note the increased number of action potentials with the 500 μs pulse indicating fiber recruitment. **I**, Synaptic efficacy (number of action potentials/stimulus frequency) was greater after increasing stimulus current duration. **J and K**, The ganglion nicotinic antagonist hexamethonium (Hex) blocked synaptically mediated action potentials demonstrating a convergence of cholinergic inputs at RAGP neurons. Scale bars are 30 μm (**A**), 1 μm (**B and C**), 0.5 μm (**D and E**), 250 μm (**F**), 50 μm (**F, inset**), and 2 min (**J**).

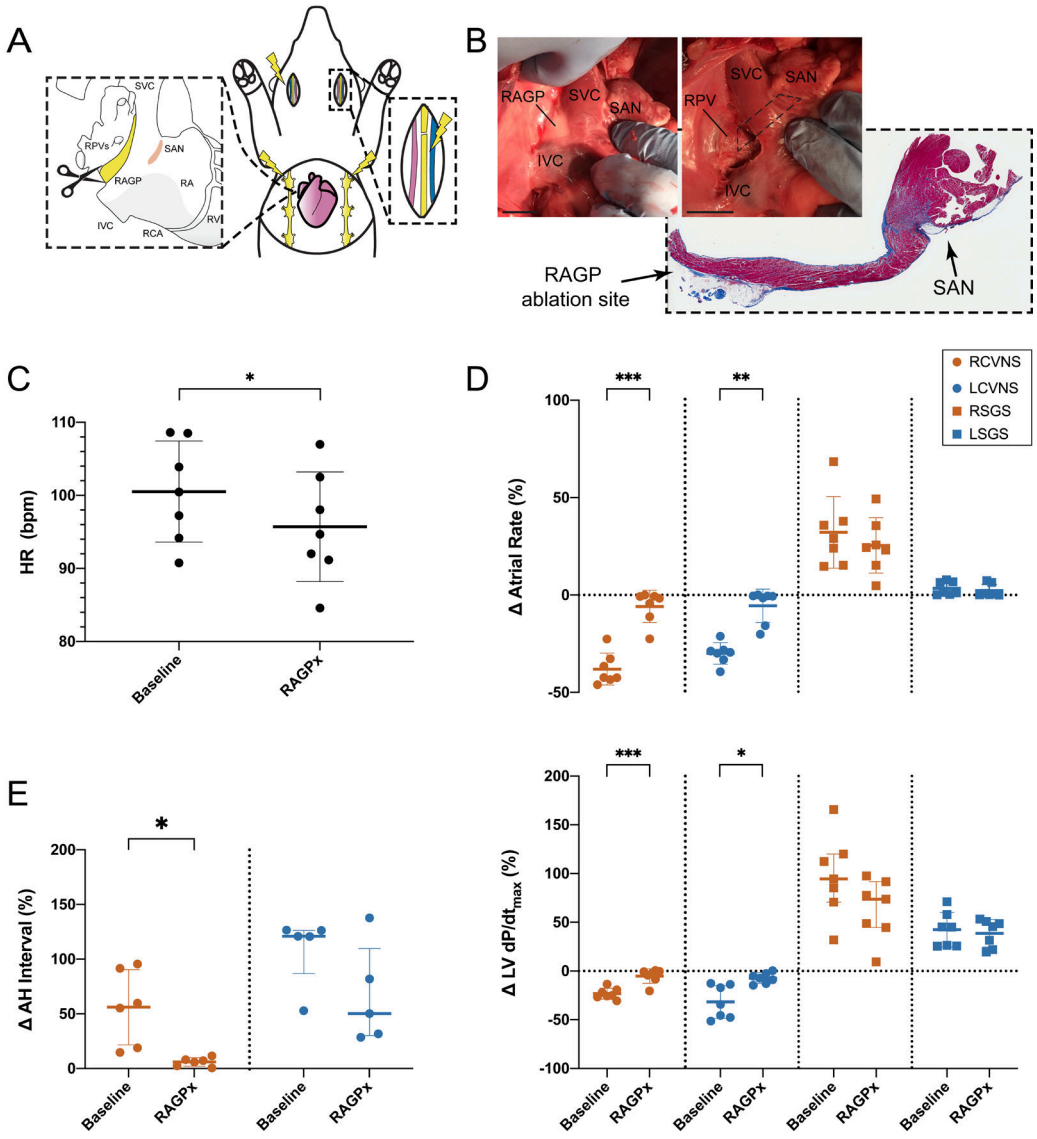

Figure 7. Ablation of the porcine right atrial ganglionated plexus (RAGP) mitigates vagal nerve stimulation (VNS)-induced bradycardia.

A, Schematic of RAGP ablation performed (n=7, 4M/3F) to assess impact of VNS- and SGS-induced changes on cardiac electrophysiology. **B**, Gross photograph of porcine RAGP before and after ablation. Representative H&E section with trichrome staining of RAGP demonstrating destruction of epicardial fat pad without impacting sinoatrial node (SAN). RAGP ablation was followed by a reduced resting heart rate (**C**; n=7) and mitigated right cervical vagal nerve stimulation (RCVNS)- and left cervical vagal nerve stimulation (LCVNS)-induced effects on atrial rate and left ventricular (LV) contractility as measured by maximal dP/dt (**D**; n=7) as well as atrial-His (AH) interval (**E**; RCVNS, n=6; LCVNS, n=5). Right stellate ganglion stimulation (RSGS)- and LSGS-induced changes in atrial rate and LV contractility were not statistically significant (**D**). Scale bars are 2 cm (**B**). Comparisons were made using paired t tests and Wilcoxon matched-pairs signed-rank tests (**C–E**). *P≤0.05, **P≤0.01, ***P≤0.001.

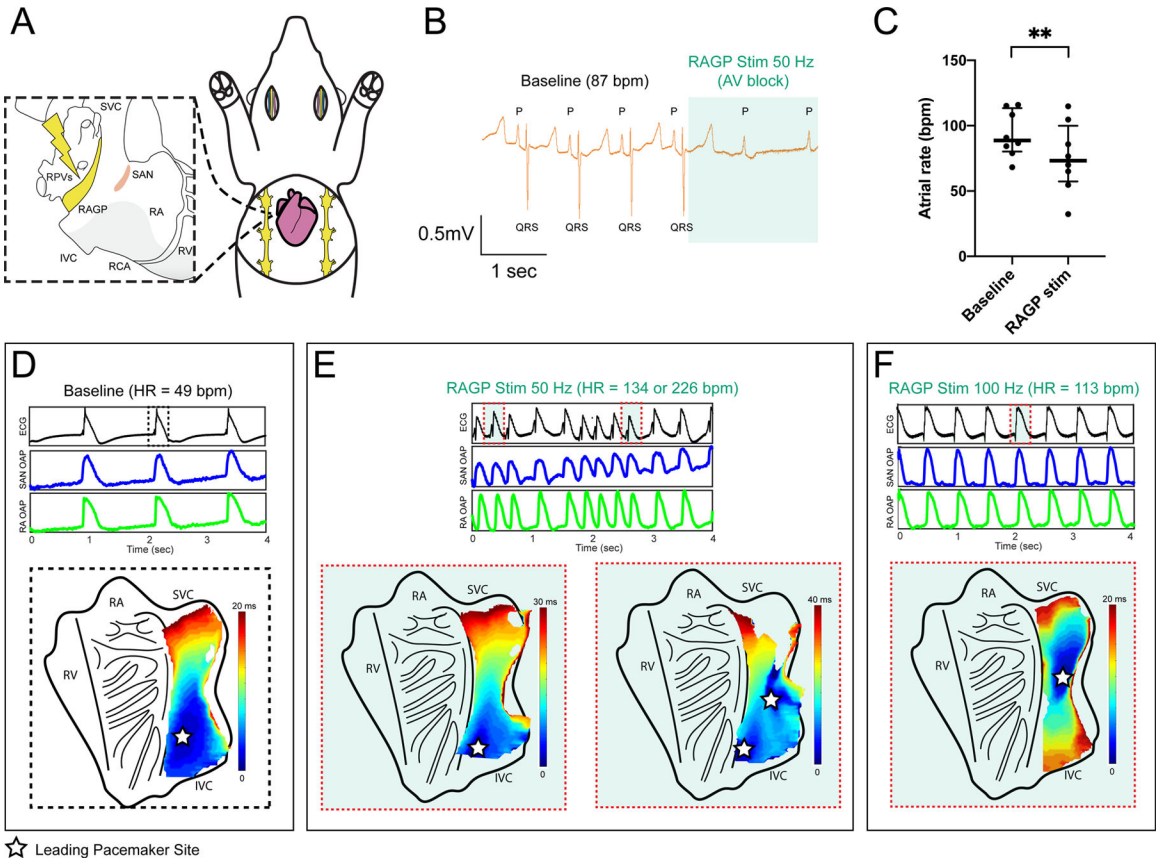

Figure 8. Stimulation of the porcine and human right atrial ganglionated plexus (RAGP) elicits sinoatrial node (SAN) rate response with pacemaker shift.

A, Schematic of in vivo porcine RAGP stimulation with multielectrode array recordings in the SAN region. **B**, ECG demonstrating significant atrial rate reduction from 87 to 61 bpm and atrioventricular (AV) block during RAGP stimulation (50 Hz, 0.1 ms, and 0.9 mA). **C**, RAGP stimulation (50 Hz, 0.1ms) caused significant sinus bradycardia from a median of 88.7 bpm (80.3–113.5) to 73.2 bpm (57.3–100.0; n=8; 6M/2F). Comparison was made using Wilcoxon matched-pairs signed-rank test, **P≤0.01. Representative optical activation maps of an ex vivo sinoatrial nodal (SAN) preparation from a 52-year-old female human donor heart before (**D**) and during (**E and F**) stimulation of the RAGP. Intrinsic firing rate of the ex vivo SAN increased from 49 bpm to at least 134 bpm at 50 Hz (**E**) and to 113 bpm with 100 Hz of stimulation (**F**). Stars indicate location of the leading pacemaker site on the endocardial side of the tissue. Corresponding ECG and optical action potential (OAP) recordings are shown below the activation maps. HR indicates heart rate; IVC, inferior vena cava; RA, right atria; RCA, right coronary artery; RPVs, right pulmonary veins; RV, right ventricle; and SVC, superior vena cava.

Major Resources Table

Animals (in vivo studies)				
Species	**Vendor or Source**	**Background Strain**	**Sex**	**Persistent ID / URL**
Pig	S&S Farms	Yucatán minipig	M+F	

Antibodies					
Target antigen	**Vendor or Source**	**Catalog #**	**Working concentration**	**Lot # (preferred but not required)**	**Persistent ID / URL**
aa 475–530 from rat VAChT	Synaptic Systems	139 103	1:500		
Native TH from rat pheocromocytoma	Millipore	AB1542	1:500		
SDS-denatured rat tyrosine hydroxylase, purified from pheochromocytoma	Pel-Freez Biologicals	P40101–150	1:1000		
Synthetic peptide (aa 1–20 from mouse VMAT2)	Synaptic Systems	138313	1:200		
Synthetic NPY coupled to bovine thyroglobulin (BTg)	ImmunoStar	22940	1:1000		
Recombinant fragment of human MAP2, aa 235–1588	Abcam	ab5392	1:1000		
Synthetic SP coupled to KLH	ImmunoStar	20064	1:1000		
Porcine VIP coupled to BTg	ImmunoStar	20077	1:1000		
Synthetic SOM coupled KLH	ImmunoStar	20067	1:1000		
aa 1423–1434 of human NOS1	Abcam	ab1376	1:1000		
Synthetic peptide to residues in Human PGP9.5	Abcam	ab108986	1:500		
S100 isolated from cow brain	Dako	GA504	1:400		
Human placental enzyme	Millipore	AB144P	1:25		
Rat CGRP C-terminal peptide, VKDNFVPTNVGSEAF	Abcam	ab36001	1:1000		
Rat alpha-CGRP	Abcam	ab81887	1:1000		
Synthetic peptide conjugated to KLH with glutaraldehyde	Sigma-Aldrich	C6219	1:800		

Data & Code Availability		
Description	**Source / Repository**	**Persistent ID / URL**
HT-qPCR data	GEO database	https://www.ncbi.nlm.nih.gov/geo/query/acc.cgi?acc=GSE149212
Blockface and acquisition images for LCM	SPARC	10.26275/56h4-ypua
Single-cell raw and processed HT-qPCR data across 4 RAGP	SPARC	10.26275/5jki-b4er
Spatially tracked transcriptomics in an RAGP	SPARC	10.26275/qkzi-b1mq

Other		
Description	**Source / Repository**	**Persistent ID / URL**